International Journal of Heat and Mass Transfer 235 (2024) 126190

Contents lists available at ScienceDirect

International Journal of Heat and Mass Transfer

journal homepage: www.elsevier.com/locate/ijhmt

Saturated pool film boiling of cryogenic fluids: Review of databases, assessment of existing models and correlations, and development of new universal correlation

Faraz Ahmad [a], Michael Meyer [b], Jason Hartwig [c], Issam Mudawar [a,b,*]

[a] Purdue University Boiling and Two-Phase Flow Laboratory (PU-BTPFL), School of Mechanical Engineering, Purdue University, 585 Purdue Mall, West Lafayette, IN 47907, USA
[b] MTS Inc., 3495 Kent Ave, West Lafayette, IN 47906, USA
[c] NASA Glenn Research Center, Fluids and Cryogenics Branch, Cleveland, OH 44135, USA

ARTICLE INFO

Keywords:
Pool film boiling
Heat transfer coefficient
Cryogens
Radiation effects
Correlations

ABSTRACT

The present study is motivated by the absence of a comprehensive pool film boiling database for cryogenic fluids. Amassing such a database is deemed essential for the thorough evaluation of existing models and correlations, simultaneously laying the groundwork for the development of new advanced predictive methodologies. To address this research gap, a Consolidated Cryogenic Pool Film Boiling Database was meticulously compiled, encompassing 1,209 data points for heat transfer coefficient (HTC) from flat surfaces across various orientations, from horizontal ($\theta = 0^{\circ}$) to vertical ($\theta = 90^{\circ}$). The exhaustive database enabled a comprehensive evaluation of prior models and correlations, revealing significant errors, particularly for elevated superheat conditions. In response, a finely tuned universal correlation for all cryogenic fluids is proposed, surpassing the predictive capabilities of its predecessors. The inclusion of a radiation term in the correlation contributes to its superior performance, especially in scenarios involving elevated temperatures, resulting in a Mean Absolute Error (MAE) of 12.94 % for the entire database, with 91.07 % of predictions falling within ±30 % of the data, and 98.92 % within ±50 %. Furthermore, outstanding performance is realized for specific orientations, with MAEs of 15.47 %, 7.92 %, 3.78 %, and 11.59 % for orientations $\theta = 0^{\circ}$, 30°, 60°, and 90°, respectively. This achievement situates the new correlation as a robust tool for thermal design and performance assessment across a diverse spectrum of devices and systems, also marking a significant advancement in understanding of cryogenic pool film boiling heat transfer phenomena.

1. Introduction

1.1. Significance of phase change processes to thermal management applications

Processes involving phase change play a crucial role in a diverse range of industrial applications, spanning both traditional and contemporary domains. Traditional applications encompass vital sectors like refrigeration and air conditioning, steam power generation, pharmaceuticals, food processing, and materials processing [1]. In these contexts, the ability to ensure predictable and reliable system operation hinges significantly on the accurate prediction of dominant interfacial behavior and the corresponding heat transfer performance.

In the realm of modern applications, the emphasis often lies in dissipating substantial heat fluxes while concurrently maintaining relatively low surface temperatures. This demand arises in various cutting-edge fields, including power electronics for hybrid vehicles, computer electronics, data centers, avionics for aircraft and spacecraft, and medical devices such as x-ray equipment [1]. The necessity for effective thermal management underscores the critical role played by an understanding of phase change phenomena, not only in conventional industries but also in the forefront of technological innovation.

The prominence of phase change methodologies stems from their remarkable efficacy in dissipating substantial heat loads, leveraging both the sensible and latent heat content inherent in the cooling fluid. The Purdue University Boiling and Two-Phase Flow Laboratory (PU-BTPFL) has been a focal point for extensive research endeavors spanning

* Corresponding author at: Purdue University Boiling and Two-Phase Flow Laboratory (PU-BTPFL), School of Mechanical Engineering, Purdue University, 585 Purdue Mall, West Lafayette, IN 47907, U.S.A.
E-mail address: mudawar@ecn.purdue.edu (I. Mudawar).

https://doi.org/10.1016/j.ijheatmasstransfer.2024.126190
Received 23 January 2024; Received in revised form 30 July 2024; Accepted 8 September 2024
Available online 12 September 2024

Nomenclature

A	Coefficient of $c_{p,g}\,\Delta T$ in modified latent heat of vaporization (h_{fg}') [dimensionless]
B	Coefficient of radiation term [dimensionless]
C_1	Constant in front of film boiling correlation [dimensionless]
c_p	Specific heat at constant pressure [J.kg^{-1}.K^{-1}]
$c_{p,\,f}$	Specific heat of saturated liquid [J.kg^{-1}.K^{-1}]
$c_{p,\,g}$	Specific heat of saturated vapor [J.kg^{-1}.K^{-1}]
D	Diameter [m]
g	Gravitational acceleration [m.s^{-2}]
h	Heat transfer coefficient (HTC) [W.m^{-2}.K^{-1}]
h_{fg}	Latent heat of vaporization [J.kg^{-1}]
h'_{fg}	Modified latent heat of vaporization [J.kg^{-1}], $h'_{fg} = h_{fg} + A{\cdot}c_{p,g}\Delta T$
h_{fb}	Film boiling heat transfer coefficient [W.m^{-2}.K^{-1}]
h_r	Radiation heat transfer coefficient [W.m^{-2}.K^{-1}]
k	Thermal conductivity [W.m^{-1}.K^{-1}]
L_b	Bubble length scale [m], $L_b = \left[\frac{\sigma}{g(\rho_f-\rho_g)}\right]^{\frac{1}{2}}$
L_x	Characteristic length, [m], $L_x = L_b$ for flat plate
m	Exponent in film boiling correlation [dimensionless]
Nu	Nusselt number; $Nu = \frac{hL_x}{k_g}$
p	Pressure [N.m^{-2}]
p_{atm}	Atmospheric pressure [N.m^{-2}]
p_{crit}	Critical pressure [N.m^{-2}]
P_R	Reduced pressure; $P_R = \frac{p}{p_{crit}}$
Pr	Prandtl number; $Pr = \mu c_p/k$
q	Heat flow rate [W]
q''	Heat flux per unit surface area [W.m^{-2}]
Ra	Rayleigh number [dimensionless], $Ra = \frac{L_x^3\rho_g(\rho_f-\rho_g)g}{\mu_g^2}\left(\frac{\mu c_p}{k}\right)_g$
T	Temperature [K]
T_{crit}	Critical temperature [K]
T_R	Reduced temperature; $T_R = \frac{T\ [K]}{T_{crit}\ [K]}$
T_{sat}	Saturation temperature [K]
ΔT_{sat}	Wall superheat, difference between wall temperature and saturation temperature of liquid [K]; $\Delta T_{sat} = T_w - T_{sat}$
T_w	Heated wall temperature [K]

Greek symbols

α	Percentage of predictions within ±30 % of the data
β	Percentage of predictions within ±50 % of the data
θ	Orientation angle of heated surface [°]
μ	Dynamic viscosity [Pa.s]
λ	Wavelength [m]
λ_c	Critical wavelength [m], $\lambda_c = 2\pi\sqrt{\frac{\sigma}{g(\rho_f-\rho_g)}}$
ρ	Density [kg.m^{-3}]
σ	Surface tension [N.m^{-1}]
σ_b	Stefan-Boltzmann constant [5.67 × 10^{-8} W/m^2.K^4]

Subscripts

atm	Atmospheric
b	Bubble
crit	Critical
Exp	Experimental (measured)
f	Saturated liquid
fb	Film boiling
g	Saturated vapor
Pred	Predicted (Calculated)
sat	Saturation
w	Heating wall

Acronyms

CFD	Computational fluid dynamics
CHF	Critical heat flux
HTC	Heat transfer coefficient
LAr	Liquid argon
LCH_4	Liquid methane
LH_2	Liquid hydrogen
LN_2	Liquid nitrogen
LO_2	Liquid oxygen
MAE	Mean absolute error
MHF	Minimum heat flux
ONB	Onset of nucleate boiling
PU-BTPFL	Purdue University Boiling and Two-Phase Flow Laboratory

over three decades, with a primary focus on realizing the advantages offered by phase change processes. The investigations conducted at PU-BTPFL encompass a diverse array of schemes, ranging from capillary driven [2] pool boiling [3], falling film [4], macro-channel flow [5], mini/micro-channel flow [6], jet impingement [7], and spray [8], to hybrid approaches that merge the strengths of combined cooling schemes [9,10].

Throughout the published phase change works, many approaches have been employed to predict the heat transfer characteristics. Firstly, the experimental approach involves the development of empirical correlations, exemplified by works such as [11-14]. Secondly, the computational avenue, as demonstrated by [15–18], provides insights through simulation techniques. Lastly, the theoretical approach, exemplified by works such as [19], contributes to a comprehensive understanding of the underlying principles governing two-phase fluid flow and heat transfer. This diverse research approach underscores the commitment to advancing knowledge and applications in the realm of phase change phenomena.

1.2. Unique physics of cryogens and their applications

Cryogenic fluids, distinguished by their extraordinarily low saturation temperatures, represent a distinct class of substances, setting them apart from conventional fluids like water and common refrigerants. The distinctive nature of cryogens compared to other fluid classes based on saturation temperature (using REFPROP 10 [20]) was recently presented by Ganesan et al. [21]. They conducted an extensive comparative analysis across various coolant classes, unveiling profound disparities in certain properties of saturated liquids. These properties encompass density (ρ_f), specific heat at constant pressure ($c_{p,f}$), thermal conductivity (k_f), viscosity (μ_f), Prandtl number (Pr_f), vapor density (ρ_g), latent heat of vaporization (h_{fg}), and surface tension (σ). They mentioned that cryogens feature low values of ρ_f, ρ_g, μ_f, and σ, and

Table 1
Critical pressure and temperature of cryogenic fluids addressed in the present study.

Cryogen	Critical Temperature [K]	Critical Pressure [MPa]
LHe	5.1953	0.22832
LH_2	33.145	1.2964
LN_2	126.192	3.3958
LAr	150.687	4.863

elevated $c_{p,f}$, and exhibit unique thermophysical behavior, with Liquid Helium (LHe) manifesting the most conspicuous departures from conventional fluids. For a comprehensive overview, please refer to Table 1 for critical temperature and pressure data pertaining to the cryogenic fluids considered in the present study.

The distinct thermophysical characteristics exhibited by cryogens pose substantial challenges, particularly in the realm of temperature measurements. This becomes especially apparent when we assess parameters such as wall superheat ($T_w - T_{sat}$) or the temperature differential between the wall and the fluid ($T_w - T_f$), where values frequently approach or descend below 0.5 K. In such scenarios involving cryogens, temperature measurement uncertainties can lead to misleading trends in heat transfer coefficient data, occasionally resulting in artificial spikes or unphysical sub-zero values. It is, therefore, of paramount importance for researchers to remain vigilant regarding the potential for significant uncertainties when interpreting cryogenic data. Our exploration of the challenges associated with temperature measurements yields two crucial insights: firstly, researchers must consistently acknowledge the likelihood of substantial uncertainties when analyzing cryogenic data, and secondly, these uncertainties can introduce notable variations when attempting to establish correlations based on experimental data.

Cryogenic fluids, due to their distinctive thermophysical characteristics, exert a significant impact across various fields, permeating numerous applications that have a lasting effect on our everyday experiences. Liquid Nitrogen (LN_2), for instance, plays an indispensable role in flash-freezing food products, preserving biological tissues and blood for medical purposes, and enabling precise cryosurgical procedures. Liquid Oxygen (LO_2) assumes a critical role in the medical arena, supporting life-sustaining systems and contributing to oxygen therapy. Additionally, cryogenic fluids play an essential part in the field of space exploration and related endeavors.

Within this context, cryogens such as LO_2, LH_2, Liquid Methane (LCH_4), and Liquid Helium (LHe) become vital assets. Liquid Helium (LHe) in particular, serves a pivotal function in maintaining the low temperatures required for space-based experiments, as well as cooling telescopes and satellites in Earth's orbit. Combinations of LO_2 with either LCH_4 or LH_2 are harnessed in ascent stages, descent stages, and in-space fuel depots, facilitating the journey to the cosmos. Liquid Hydrogen (LH_2) emerges as an indispensable component in nuclear thermal propulsion systems and has garnered attention for its potential integration within advanced propulsion systems, serving a dual role as both propellant and coolant.

1.3. Background physics of pool boiling

Pool boiling, a rather simple and economical scheme, proves to be highly effective for achieving efficient two-phase cooling. Its versatility makes it suitable for widespread application in various industrial sectors, encompassing both low-temperature and high-temperature scenarios. In low-temperature settings, such as electronic component cooling, power device regulation, and superconductor coil maintenance, pool boiling is extensively utilized. This method takes advantage of the impressive latent heat capacity of the coolant, effectively dissipating significant amounts of heat. As a result, device temperatures are kept well below critical thresholds, primarily determined by material integrity and device reliability considerations. Conversely, in high-temperature applications, pool boiling is commonly employed for the quenching of metal alloy parts during heat treating processes. The primary objective in this context is to achieve an optimal microstructure within the alloy, thereby enhancing its mechanical properties. This dual capability of pool boiling, spanning from low to elevated temperatures, underscores its adaptability and efficiency in meeting diverse industrial cooling needs.

Researchers often delve into comprehending the diverse mechanisms and stages of pool boiling by referring to the boiling curve. This curve, a fundamental tool in the study of pool boiling, is typically derived through two distinct measurement methods: the *steady-state heating method* and the *transient (quenching) method*. The preference for the steady-state heating method in pool boiling studies stems from its superior accuracy in measuring crucial heat transfer parameters. When employing the steady-state heating method, the boiling curve is constructed through a series of steps, starting from zero power and gradually adjusting the wall heat flux in small increments. Following each increment, a sufficient waiting period is observed to ensure the attainment of a stable wall temperature before measurement. Alternatively, quenching entails preheating the wall to a temperature within the film boiling region and promptly cooling it in a liquid. This procedure generates a temperature-time (quench) curve, encapsulating all distinct boiling regions, including transition boiling. It is crucial to recognize that the quench curve is highly dependent on thermal mass of the wall. Ultimately, the analysis of transient wall conduction, often employing a lumped capacitance model, determines the variation of heat flux with wall superheat for each boiling region.

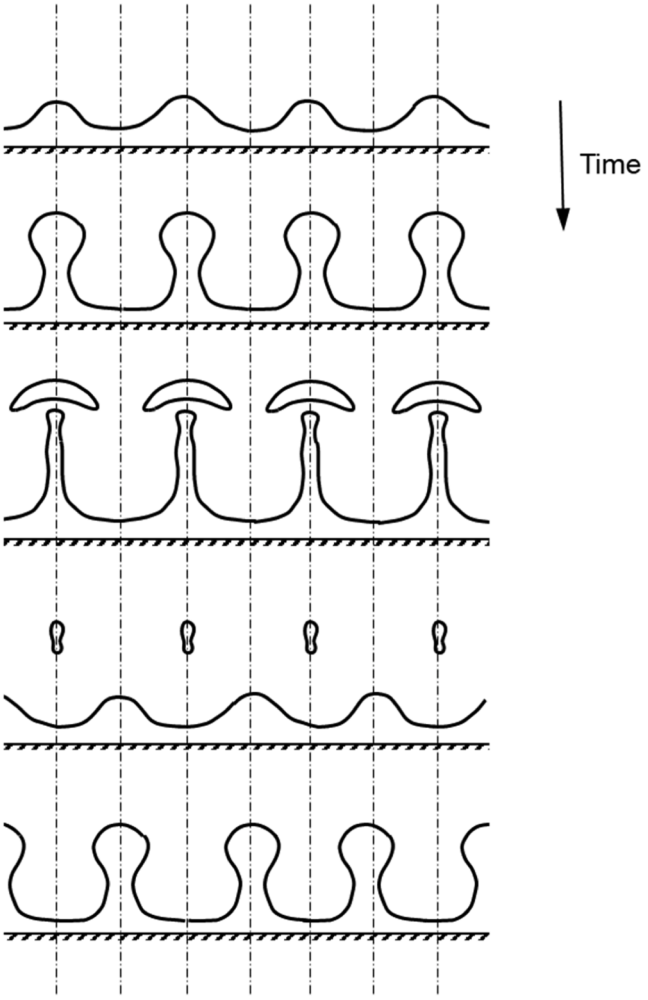

Fig. 1. Schematic of the liquid-vapor interface during stable pool film boiling on a flat infinite horizontal heating surface.

1.4. Mechanisms of pool film boiling

In the context of saturated pool film boiling, specifically on a horizontal flat surface where wall temperatures exceed the minimum heat flux (MHF) point temperature, a distinct instability pattern emerges at the vapor-liquid interface, coupled with a vapor release mechanism. Fig. 1 presents a schematic representation of the liquid-vapor interface during stable film boiling on an infinite horizontal surface. When the

wall temperature surpasses that corresponding to the MHF point, a thin and continuous vapor film forms between the heating surface and the bulk saturated liquid, preventing direct liquid contact. Heat conduction from the heating surface across the vapor film induces a phase change at the liquid-vapor interface. The influence of gravity, opposed by surface tension, introduces instability along the interface, resulting in the formation of a wavy vapor film with peaks and valleys. This instability prompts the flow of vapor accumulated beneath the liquid from the valleys to two adjacent peaks, giving rise to the formation of a series of repetitive unit cells. Subsequently, significant vapor formation leads to the release of vapor from the peaks. This intricate interplay of instability and vapor release characterizes the behavior of the liquid-vapor interface during stable film boiling on a horizontal surface with temperatures surpassing the MHF point.

1.5. Parameters influencing pool film boiling

Film boiling, particularly in pool configurations, plays a pivotal role in the meticulous design of thermal management systems, despite the relatively modest heat transfer coefficients characterizing this phase on the boiling curve. Researchers consistently emphasize this aspect due to its critical role in averting potential damage to temperature sensitive devices such electronic components within the system. This emphasis arises from the emergence of the vapor film above the heating surface during the film boiling regime, effectively acting as a thermal barrier and impeding direct contact between the cooling liquid and the heating surface. Consequently, the precise prediction and understanding of film boiling behaviour become paramount in the intricate task of designing thermal systems and enhancing heat transfer coefficients. Over the past few decades, a substantial amount of research has been devoted to delving into a myriad of factors that influence the film boiling heat transfer coefficient. This comprehensive exploration encompasses a range of variables, including system pressure, the orientation angle of the heated surface, the impact of radiation arising from elevated temperatures, and the roughness of the heated surface.

For example, Class et al. [22] conducted a comprehensive investigation into the effect of *system pressure* on the heat transfer performance in LH_2 film boiling. Notably, they observed a discernible increase in the heat transfer coefficient (HTC) with increasing pressure. Kumar et al. [23] observed a similar correlation between the HTC and system pressure in their numerical investigation. In their study on LN_2, they found that an increase in system pressure at a constant wall superheat led to a decrease in bubble height. However, the pressure variation had no significant impact on bubble departure rate, except at very high pressures. In contrast to nucleate pool boiling, where the impact of pressure has been a subject of thorough investigation by numerous researchers, the film boiling regime has not received comparable attention regarding pressure effects.

Expanding on the outcomes reported by Class et al. [22], their findings indicated an augmentation of HTC with an increase in the *orientation angle*, transitioning from horizontal ($\theta = 0^\circ$) to vertical ($\theta = 90^\circ$). This observation aligns with the results reported by other researchers, such as Price [24], who delved into LN_2 film boiling across various inclination angles (0°, 30°, 60°, 90°). Price's study also revealed that an increase in the inclination angle yields higher HTCs. One interesting aspect highlighted by Price is the monotonous nature of the increase in HTCs with increasing orientation angle. This monotonic trend not only adds a degree of predictability to the behaviour but also facilitates the generalization of HTCs for different orientation angles, providing valuable insights for broader applications in thermal management system design. The findings of Scheiwe and Hartmann [25] further support the notion that vertical orientation generally leads to superior HTCs compared to horizontal orientation.

Due to the comparatively elevated wall superheat associated with film boiling, it becomes imperative to consider *radiation heat transfer* as a significant factor. Despite the critical importance of this term, it has consistently been overlooked by previous researchers, potentially owing to the inherent challenges associated with determining surface emissivity. Surface emissivity is a complex parameter influenced by various factors such as temperature, oxidation, and surface roughness, among others, making its incorporation challenging. Nevertheless, some researchers advocate for the inclusion of radiation in the analysis of the film boiling region. For instance, in a study on LN_2 film boiling, Sauer and Ragsdell [26] emphasized that radiation heat transfer cannot be disregarded, particularly in stable film boiling conditions where wall superheat can reach temperatures ranging from 500 to 1200 K. This assertion is corroborated by Brentari and Smith [27] who, based on their experimental findings, developed a new correlation building upon Berenson's [28] earlier correlation. Similarly, Price [24] conducted a comparative analysis of experimental results with the correlations proposed by Berenson [28] and Chang [29], concluding that absence of a radiation term in these correlations contributed to a consistent underestimation of experimental results. In response, he modified the coefficient of Berenson's correlation using the experimental values of Brentari and Smith for LN_2. Overall, these insights prompt a need to re-evaluate most existing correlations and underscore the importance of a comprehensive understanding of the role of radiation in film boiling scenarios.

Class et al. [22], in his study mentioned above, also investigated the influence of *surface roughness* on HTC in the film boiling regime for LH_2. Overall, they concluded that the impact of surface roughness is nearly negligible, presumably because surface roughness features are buried well within the vapor film. This finding may explain why many researchers have refrained from exploring the influence of surface roughness on film boiling HTC. In contrast, nucleate pool boiling has seen widespread investigation into the effect of surface roughness, with a consensus among authors that increasing surface roughness has a positive effect on the HTC of nucleate pool boiling.

1.6. Inferences drawn from literature review

Building upon the concise literature review outlined above and the detailed discussion of prior models and correlations to follow, several noteworthy conclusions have surfaced. The most salient of these are as follows:

1. In the pool film boiling regime, the behavior of the HTC is notably dependent on fewer variables that nucleate pool boiling. Importantly, the impact of specific parameters on HTC tends to be rather monotonic, simplifying prediction and allowing for the generalization of their effects in the film boiling region.
2. A distinct dissimilarity between nucleate pool boiling and film pool boiling lies in the influence of surface roughness. In nucleate pool boiling, the impact of this parameter on HTC is both significant and complex, varying with heat flux, fluid properties, surface material, and orientation. Conversely, in film boiling, surface roughness has minimal, if any, significant impact on HTC.
3. The orientation angle of a flat heated surface significantly affects the heat transfer performance in film boiling. Unlike nucleate pool boiling, the effect of orientation angle on the film boiling HTC is monotonic, which facilitates systematic utilization of this factor for HTC predictions.
4. In the film boiling regime, relatively high wall temperatures necessitate consideration of radiation heat transfer effects, especially above 400 K, as is the case with LN_2.
5. Like the nucleate boiling regime, pressure has significant influence on HTC in the film boiling regime. However, this influence has not received adequate attention in most experimental works.

1.7. Objectives of the present study

The ongoing investigation constitutes a crucial component of initiatives aimed at crafting predictive tools for the design and performance

evaluation of cryogenic systems integral to propellant storage, transfer, generation, conveyance, and utilization. A particular emphasis is placed on reinforcing the in-situ resource utilization (ISRU) objectives outlined by the National Aeronautics and Space Administration (NASA). These endeavors span a diverse spectrum of applications, scales, and environments, aligning seamlessly with NASA's upcoming missions to both the Moon and Mars.

More precisely, the focus of this study is to contribute to the formulation of detailed heat transfer relations for each segment and transition point along the boiling curve for cryogens. This is indispensable for constructing a comprehensive boiling curve, ranging from the film boiling region to the single-phase liquid cooling region. Notably, the present PU-BTPFL team, in collaboration with the NASA Glenn Research Center, has already published new critical heat flux (CHF) correlations [30], as part of these efforts.

The ongoing investigation distinctly enhances our technical comprehension by specifically focusing on the prediction of heat transfer in the film boiling region. This targeted analysis is centered on saturated pool boiling from flat surfaces, considering orientations ranging from horizontal to vertical and those in between.

In summary, the primary objectives of this study can be outlined as follows:

i. Undertake a comprehensive review of existing models and correlations pertaining to the pool film boiling region.
ii. Assemble a new Consolidated Cryogenic Pool Film Boiling Database (referred to hereafter as the Consolidated Database) encompassing different cryogens (LHe, LH_2, LAr, and LN_2) from reputable worldwide sources.
iii. Evaluate the accuracy of prior models and correlations by comparing predictions against the Consolidated Database.
iv. Recognizing that most existing models are tailored for non-cryogenic fluids, and may not offer accurate predictions for cryogens, propose modifications to prior formulations to enhance accuracy specifically for cryogenic applications.
v. Investigate parametric trends within the Consolidated Database to identify gaps in the ranges of key parameters, providing a foundation for recommending future experimental work.
vi. Propose a new correlation capable of accurately predicting the film boiling heat transfer characteristics for different cryogens.

2. Review of prior pool film boiling models and correlations

Numerous endeavors by researchers have been undertaken to conceptualize the intricacies of heat transfer mechanisms in film boiling. Scholarly discourse among prior works is categorized into three primary segments, delineated by the distinct geometries under investigation: film boiling on wires and cylindrical bodies, film boiling on flat plates, and film boiling on spherical bodies. The genesis of the first two categories can be traced back to seminal analytical models crafted for film boiling, specifically one devised by Bromley [31] for a horizontal cylinder or tube, and another by Berenson [28] (see also [32]) for a horizontal plate.

Bromley [31] pioneered his model for pool film boiling, primarily focusing on horizontal tube. Nevertheless, he extended the applicability of his findings to encompass a vertical tube and vertical plate through judicious employment of geometric transformations. Employing a synthesis of geometrical, mechanistic, and thermophysical relationships, he formulated his analytical model for the HTC in film boiling by drawing inspiration from the seminal work of Nusselt [33] on film condensation on vertical surfaces. Additionally, Bromley [31] delved into the consideration of radiation heat transfer effects for specific fluids. However, he acknowledged his inability to resolve the coupled effects between convective and radiative heat transfer in his model, rendering his solution subsequently proven inaccurate. Notably, certain results derived by Bromley [31] exhibit discrepancies of 30–100 %, particularly under conditions of elevated superheat and both very small or very large diameters.

Subsequent to the examination conducted by Bromley, a number of researchers endeavored to rectify the constraints inherent in his model. Noteworthy is the work of Nishikawa et al. [34], who scrutinized the impact of inertial forces. Their approach involved postulating velocity and temperature profiles within the vapor film, culminating in a semi-empirical correlation derived from meticulous utilization of experimental data. Their conclusion posited that the most accurate representation of physical behavior arises from assuming zero velocity at the interface and a quadratic temperature profile. Bromley's model, confined to tube diameters falling within an intermediate range determined by ratio of tube diameter to the Taylor wavelength, prompted the scrutiny of Breen and Westwater [35]. In a bid to surmount this limitation, they investigated the repercussions of varying cylinder diameters. The delineation of cylinder diameters into three distinct ranges, guided by the most-dangerous wavelength of Taylor instability, unveiled a nuanced understanding. They proposed that for intermediate diameters, Bromley's model retained its applicability, while for larger sizes, the HTC was completely independent of diameter. And, for minuscule diameters, such as for wires, heat flux exhibited independence from wire diameter, implying the heat transfer rate is limited by the bubble release mechanism. In an expansive refinement of Bromley's framework, Sciance et al. [36] broadened its applicability across an extended spectrum of operating temperatures. Their augmentation involved incorporating the contribution of reduced temperature, denoted as $T_R = T_{sat}/T_{crit}$, enhancing the model's capacity for precise curve-fitting of data points. Meanwhile, Sakurai et al. [37,38] elevated Bromley's exploration of radiation effects by introducing considerations for liquid subcooling, specifically delving into the liquid thermal boundary layer. This extension was subjected to rigorous validation against experimental data, conducted with high emissivity cylinders.

Film boiling on a horizontal flat surface exhibits nuanced characteristics distinct from those observed on a horizontal cylinder. In contrast to Bromley's formulation, Berenson [28] directed his effort towards fashioning a model tailored for film boiling on a horizontal plate. The crux of disparity between the two modeling approaches resides in the incorporation of the Taylor instability in the latter. Berenson depicted the film boiling behavior as one consisting of repeated cells centered within each is a large vapor release dome surrounded by a thin horizontal radial vapor film, with the cell's diameter dictated by the most-dangerous Taylor wavelength, λ_c. Berenson posited the existence of radial vapor inflow from the thin film toward the central dome propelled by the hydrostatic pressure differential between the vapor dome and the film. He also used the assumption that heat transfer occurs exclusively through the thin film portion of the cell and is governed solely by heat conduction. The model culminated in an expression for vapor film thickness, which served as the basis for calculating the HTC across the vapor film. Berenson's model underwent meticulous validation against previously collected data, revealing a commendable ± 10 % error in the proximity to the MHF point. Building on this success, he harnessed his formulation to ascertain the minimum temperature requisite for instigating film boiling, thereby endeavoring to delineate the MHF point.

Acknowledging the limitations inherent in Berenson's model, several researchers have undertaken endeavors to refine and enhance its efficacy. Notably, Baumeister and Hamill [39,40] approached the phenomenon with a nuanced perspective. Commencing with the same geometric simplification featuring the vapor dome enveloped by a thin annular vapor film in a repetitive pattern, they cast the predicament as an optimization challenge. In this framework, they determined optimal values for the radius of the vapor dome and the outer cell radius, grounding their rationale with the maximization of entropy generation by invoking the second law of thermodynamics. While their analytical formulation exhibited subtle deviations from Berenson's, their final expression is only slightly different from that of Berenson's. In a departure from the geometric assumptions of Berenson, Frederking et al.

Table 2
Models and Correlations for pool film boiling heat transfer, in chronological order.

No.	Year	Author(s)	Correlation	Geometry
1	1949	Bromley [31]	$h_{fb} = \frac{k_g}{L_x} C_1 \left[Ra_{L_x} \left(\frac{h'_{fg}}{c_{p,g}\Delta T} \right) \right]^m$ $L_x = D,\ C_1 = 0.62,\ m = 0.25$ $h'_{fg} = h_{fg} + 0.5\ c_{p,g}\Delta T$	Horizontal tubes
2	1958	Hsu & Westwater [49]	$h_{fb} = \frac{k_g}{L_x} C_1 \left[Ra_{L_x} \left(\frac{h'_{fg}}{c_{p,g}\Delta T} \right) \right]^m$ $L_x = L,\ m = 0.25$ $C_1 = 0.667$ *if liquid is stagnant* $C_1 = 0.943$ *ifliquid is moving with same velocity as vapor* $h'_{fg} = h_{fg} + 0.4\ c_{p,g}\Delta T$ L is tube length, ranging from 6.5 to 16.5 cm	Vertical tubes
3	1957	Chang [50]	$h_{fb} = \frac{k_g}{L_x} C_1 \left[Ra_{L_x} \left(\frac{h'_{fg}}{c_{p,g}\Delta T} \right) \right]^m$ $L_x = L_b,\ C_1 = 0.278,\ m = \frac{1}{3}$ $h'_{fg} = h_{fg} + 0.5\ c_{p,g}\Delta T$	Horizontal and vertical plates
4	1959	Kutateladze [51]	$h_{fb} = \frac{k_g}{L_x} C_1 \left[Ra_{L_x} \left(\frac{h'_{fg}}{c_{p,g}\Delta T} \right) \right]^m$ $L_x = L,\ C_1 = \frac{4}{3} c_{11} \left(\frac{1}{\psi} \right)^{0.25},\ m = 0.25$ $0.53 < c_{11} < 0.72$ $\psi = 1 + \frac{h_r \delta_g}{k_g}$ $h'_{fg} = h_{fg} + 0.5\ c_{p,g}\Delta T$	Vertical plates; parameter ψ accounts for radiation effects
5	1961	Berenson [28]	$h_{fb} = \frac{k_g}{L_x} C_1 \left[Ra_{L_x} \left(\frac{h'_{fg}}{c_{p,g}\Delta T} \right) \right]^m$ $L_x = L_b,\ C_1 = 0.425,\ m = 0.25$ $h'_{fg} = h_{fg} + 0.5\ c_{p,g}\Delta T$	Horizontal tubes
6	1962	Breen & Westwater [35]	$h_{fb} = \frac{k_g}{L_x} C_1 \left[Ra_{L_x} \left(\frac{h'_{fg}}{c_{p,g}\Delta T} \right) \right]^m$ $L_x = L_b,\ C_1 = 0.37 + 0.28 \sqrt{\frac{\sigma}{gD^2(\rho_f - \rho_g)}},\ m = 0.25$ $h'_{fg} = h_{fg} + 0.5\ c_{p,g}\Delta T$	Horizontal tubes and wires
7	1963	Frederking & Clark [45]	$h_{fb} = \frac{k_g}{L_x} C_1 \left[Ra_{L_x} \left(\frac{h'_{fg}}{c_{p,g}\Delta T} \right) \right]^m$ $L_x = D,\ C_1 = 0.14,\ m = \frac{1}{3}$ $h'_{fg} = h_{fg} + 0.5\ c_{p,g}\Delta T$	Spheres and horizontal tubes
8	1964	Pomerantz [52]	$h_{fb} = \frac{k_g}{L_x} C_1 \left[Ra_{L_x} \left(\frac{h'_{fg}}{c_{p,g}\Delta T} \right) \right]^m$ $L_x = D,\ C_1 = 0.62 \left(\frac{D}{\lambda_c} \right)^{0.172},\ m = 0.25$ $\lambda_c = 2\pi \sqrt{\frac{\sigma}{g(\rho_f - \rho_g)}}$ $h'_{fg} = h_{fg} + 0.5\ c_{p,g}\Delta T$	Horizontal tubes
9	1964	Merte & Clark [46]	$h_{fb} = \frac{k_g}{L_x} C_1 \left[Ra_{L_x} \left(\frac{h'_{fg}}{c_{p,g}\Delta T} \right) \right]^m$ $L_x = D,\ C_1 = 0.15,\ m = \frac{1}{3}$ $h'_{fg} = h_{fg} + 0.5\ c_{p,g}\Delta T$	Spheres
10	1966	Frederking et al. [41]	$h_{fb} = \frac{k_g}{L_x} C_1 \left[Ra_{L_x} \left(\frac{h'_{fg}}{c_{p,g}\Delta T} \right) \right]^m$ $L_x = L_b,\ C_1 = 0.2, m = 0.25$ $h'_{fg} = h_{fg} + 0.5\ c_{p,g}\Delta T$	Spheres
11	1966	Heath & Costello [53]	$h_{fb} = \frac{k_g}{L_x} C_1 \left[Ra_{L_x} \left(\frac{h'_{fg}}{c_{p,g}\Delta T} \right) \right]^m$ $L_x = w,\ C_1 = 0.425 \left[\frac{2\pi g}{\lambda_c} \frac{a}{g} \frac{w}{w_B} \right]^{0.25},\ m = 0.25$ $h'_{fg} = h_{fg} + 0.5\ c_{p,g}\Delta T$ w is width of the heater and w_B is the width of Berenson's heater	Vertical strip heater
12	1967	Sciance et al. [36]	$h_{fb} = \frac{k_g}{L_x} C_1 \left[Ra_{L_x} \left(\frac{h'_{fg}}{c_{p,g}\Delta T} \right) \right]^m$ $L_x = L_b,\ C_1 = 0.346\ T_r^{-0.552},\ m = 0.276$ $L_b = \sqrt{\frac{\sigma}{g(\rho_f - \rho_g)}}$ $T_R = \frac{T\ [K]}{T_{crit}\ [K]}$ $h'_{fg} = h_{fg} + 0.5\ c_{p,g}\Delta T$	Horizontal tubes

(*continued on next page*)

Table 2 (*continued*)

No.	Year	Author(s)	Correlation	Geometry
13	1967	Flanigan [54]	$h_{fb} = a_2\left(\frac{1}{L_x} + C\right)Pr_g^{\frac{1}{4}}$ $C = \frac{1437}{m}$ $a_2 = 13.38 - 15.53T_R + 6.14T_R^2 - 0.588T_R^3$ $T_R = \frac{T\ [K]}{T_{crit}\ [K]}$	Horizontal tubes
14	1967	Baumeister & Hamill [39]	$h_{fb} = \frac{k_g}{L_x}C_1\left[Ra_{L_x}\left(\frac{h'_{fg}}{c_{p,g}\Delta T}\right)\right]^m$ $L_x = L_b,\ \ C_1 = 0.373\left[1 + \frac{9}{\sqrt{6}}\frac{L_b}{D_o} + \frac{8}{3\sqrt{6}}\left(\frac{L_b}{D_o}\right)^3\right]^{0.25},\ m = 0.25$ $h'_{fg} = h_{fg}\left(1 + \frac{0.34\ c_{p,g}\Delta T}{h_{fg}}\right)^2$	Horizontal tubes
15	1967	Baumeister & Hamill [40]	$h_{fb} = \frac{k_g}{L_x}C_1\left[Ra_{L_x}\left(\frac{h'_{fg}}{c_{p,g}\Delta T}\right)\right]^m$ $L_x = L_b,\ \ _1 = 0.485\left[\left(\frac{L_b}{D_o}\right)^3 + 2.25\left(\frac{L_b}{D_o}\right)\Delta^2\right]^{0.25},\ m = 0.25$ For $\frac{L_b}{D_o} < 3$: $\Delta\ = 1$ For $3 < \frac{L_b}{D_o} < 10$: $\Delta\ = \exp\left[4.35\left(\frac{k_g\mu_g\Delta T}{D\rho_g\sigma g h'_{fg}}\right)^{0.25}\right]$ For $\frac{L_b}{D_o} > 10$: $C_1\ = 0.35\left(\frac{L_b}{D_o}\right)^{\frac{3}{4}}$ $h'_{fg} = h_{fg}\left(1 + \frac{0.34\ c_{p,g}\Delta T}{h_{fg}}\right)^2$	Horizontal tubes
16	1971	Sauer & Ragsdell [26]	$h_{fb} = \frac{k_g}{L_x}C_1\left[Ra_{L_x}\left(\frac{h'_{fg}}{c_{pg}\Delta T}\right)\right]^m$ $L_x = L_b,\ \ C_1 = 0.512,\ m = 0.25$ $h'_{fg} = h_{fg} + 0.4\ c_{p,g}\Delta T$	Horizontal plates
17	1972	Clements & Colver [55]	$h_{fb} = \frac{k_g}{L_x}C_1\left[Ra_{L_x}\left(\frac{h'_{fg}}{c_{p,g}\Delta T}\right)\right]^m$ $L_x = D,\ \ C_1 = 0.94\left(\frac{T_{crit}}{T_{sat}}\right)^2,\ m = 0.25$ $h'_{fg} = h_{fg} + 0.5\ c_{p,g}\Delta T$	All geometries
18	1978	Farahat [48]	$h_{fb} = \frac{k_g}{L_x}C_1\left[Ra_{L_x}\left(\frac{h'_{fg}}{c_{p,g}\Delta T}\right)\right]^m$ $L_x = D,\ \ C_1 = 0.18,\ m = \frac{1}{3}$ $h'_{fg} = h_{fg} + 0.5\ c_{p,g}\Delta T$	Spheres
19	1981	Kida et al. [56]	$h_{fb} = \frac{k_g}{L_x}C_1\left[Ra_{L_x}\left(\frac{h'_{fg}}{c_{p,g}\Delta T}\right)\right]^m$ $L_x = \lambda_c,\ \ C_1 = 0.75 + 0.032\frac{\lambda_c}{D},\ m = 0.25$ $\lambda_c = 2\pi\sqrt{\frac{\sigma}{g(\rho_f - \rho_g)}}$ $h'_{fg} = h_{fg}\left(1 + \frac{0.34\ c_{p,g}\Delta T}{h_{fg}}\right)^2$	Horizontal wires
20	1981	Klimenko [42]	Laminar: $\left(\frac{g\rho_g(2\pi L_x)^3(\rho_f - \rho_g)}{\mu_g^2} < 10^8\right)$ $h_{fb} = 0.19f\frac{k_g}{L_x}\left[\frac{g\rho_g(2\pi L_x)^3(\rho_f - \rho_g)}{\mu_g^2}\right]^{\frac{1}{3}}Pr_f^{\frac{1}{3}}$ For $\left(\frac{h_{fg}}{c_{p,g}\Delta T}\right)^{\frac{1}{3}} \le 1.4$: $f = 1$ For $\left(\frac{h_{fg}}{c_{p,g}\Delta T}\right)^{\frac{1}{3}} > 1.4$: $f = 0.89\left(\frac{h_{fg}}{c_{p,g}\Delta T}\right)^{\frac{1}{3}}$ Turbulent: $\left(\frac{g\rho_g(2\pi L_x)^3(\rho_f - \rho_g)}{\mu_g^2} > 10^8\right)$ $h_{FB} = 0.0086f\frac{k_g}{L_x}\left[\frac{g\rho_g(2\pi L_x)^3(\rho_f - \rho_g)}{\mu_g^2}\right]^{\frac{1}{2}}Pr_f^{\frac{1}{3}}$ For $\left(\frac{h_{fg}}{c_{p,g}\Delta T}\right)^{\frac{1}{3}} \le 2$: $f = 1$ For $\left(\frac{h_{fg}}{c_{p,g}\Delta T}\right)^{\frac{1}{3}} > 2$: $f = 0.71\left(\frac{h_{fg}}{c_{p,g}\Delta T}\right)^{\frac{1}{2}}$	Horizontal plates

(*continued on next page*)

Table 2 (*continued*)

No.	Year	Author(s)	Correlation	Geometry
21	1990	Sakurai et al. [37,38]	$h_{fb} = \frac{k_g}{L_x} C_1 \left[Ra_{L_x} \left(\frac{h'_{fg}}{c_{p,g}\Delta T} \right) \right]^m$ $L_x = D, \quad C_1 = 0.612 \left[\frac{E^3}{1 + \frac{E}{S_p Pr_f}} \right]^{0.25}, \quad m = 0.25$ $E = \left(A + C\sqrt{B}\right)^{\frac{1}{3}} + \left(A - C\sqrt{B}\right)^{\frac{1}{3}} + \frac{1}{3} S_c$ $A = \frac{1}{27} S_c^3 + \frac{1}{3} R^2 S_p Pr_f S_c + \frac{1}{4} R^2 S_p^2 Pr_f^2$ $B = \frac{-4}{27} S_c^2 + \frac{2}{3} S_p Pr_f S_c - \frac{32}{27} R^2 S_p Pr_f + \frac{1}{4} S_p^2 Pr_f^2 + \frac{2}{27} \frac{S_c^3}{R^2}$ $C = \frac{1}{2} R^2 S_p Pr_f$ $R = \sqrt{\frac{\rho_g \mu_g}{\rho_f \mu_f}}$ $S_c = \frac{c_{p,f} \Delta T_{sub}}{h'_{fg}}, \; S_p = \frac{c_{p,f} \Delta T_{sat}}{h'_{fg} Pr_g}$ $h'_{fg} = h_{fg} + 0.5 \, c_{p,g} \Delta T$	Horizontal tubes
22	1993	Chu [57]	$h_{fb} = \frac{k_g}{L_x} C_1 \left[Ra_{L_x} \left(\frac{h'_{fg}}{c_{p,g}\Delta T} \right) \right]^m$ $L_x = L, \; m = \frac{1}{3}$ $C_1 = 1.11 C_l \left(\frac{0.5}{C_l} \right)^{\frac{4}{3}}$ $C_l = \frac{0.13 Pr_f^{0.22}}{\left[1 + 0.61 Pr_f^{0.81} \right]^{0.42}}$ $h'_{fg} = h_{fg} \left[1 + F \left(\frac{c_{p,g}\Delta T}{h_{fg}} \right) \right]$ For $\left(\frac{c_{p,g}\Delta T}{h_{fg}} \right) \ll 1$: $F = 0.5$ For $\left(\frac{c_{p,g}\Delta T}{h_{fg}} \right) \gg 1$: $F = 1$	Vertical surfaces
23	1998	Son & Dhir [58]	$h_{fb} = \frac{k_g}{L_x} C_1 \left[Ra_{L_x} \left(\frac{h_{fg}}{c_{p,g}\Delta T} + 0.5 + 1.3 \left(\frac{c_{p,g}\Delta T}{h_{fg}} \right)^{0.25} \right) \right]^m$ $L_x = L_b, \; m = \frac{1}{4}$	

- For ease of comparison, most of the above correlations are shown in a unified form that differs from how they are presented in original references.
- $\Delta T = T_w - T_{sat}$.

[41] gleaned insights from their experiments, particularly in the realm of high vapor superheat common in cryogenic fluids. They observed a transition from the cellular structure of the dome to a more chaotic arrangement. In response, they devised an alternative model that deviated from Berenson's geometrical premise. Concurrently, Klimenko [42] pinpointed a notable omission in Berenson's model – failure to account for turbulence in the vapor film. Employing Reynolds' analogy with Colburn's correction, Klimenko formulated a novel correlation, diverging in structure from the established model. Furthermore, he advocated for a more accurate incorporation of superheat within the vapor region by considering the effect of heat of vaporization. These diverse approaches collectively contribute to the ongoing refinement and evolution of models elucidating the intricate dynamics of film boiling.

The gravitational field introduces inherent instability in the system as the vapor forms beneath the denser liquid. The exploration of such hydrodynamic instability was pioneered by Chang [29] in the context of film boiling over a horizontal plate. He proposed the existence of a wavy interface between the vapor and liquid giving rise to buoyant and viscous forces within the vapor layer perpendicular to the surface. These forces, in turn, accentuate the undulating motion at the interface, ultimately leading to interfacial breakup once the spacing between wave peaks becomes equal to the critical wavelength. By estimating the critical thickness of the vapor layer at which the breakup occurs, Chang [29] postulated that it could serve as a predictive metric for the film boiling heat transfer rate. In a parallel vein, Zuber [43] identified the burnout phenomenon marking the transition from nucleate boiling to film boiling as stemming from instability induced by both buoyancy-induced Taylor instability and Helmholtz instability associated with relative velocity between the rising vapor and replenishment liquid. The endeavors of Chang and Zuber shed light on the multifaceted interfacial instability aspects of film boiling resulting from the presence of gravitational influences and relative velocity effects, contributing to a more comprehensive understanding of heat transfer phenomena in such systems.

In the realm of film boiling, the consideration of orientation has been a recurrent theme in discussions concerning various models and correlations [44]. Notably, when addressing spherical objects, symmetry renders orientation inconsequential. Pioneering work in developing correlations for film boiling on a spherical object was undertaken by Frederking and Clark [45]. Their analytical model involved the simplifying assumption of vapor film thickness much smaller than the sphere's radius and ignoring the influences of inertia, convection, and radiation. A key observation from their work is that the film boiling HTC is virtually independent from the heater geometry. This significant conclusion was substantiated through a comparative analysis, juxtaposing the results of Merte and Clark [46] for film boiling on a sphere with those of Ruzicka [47] for vertical tubes. Building upon this foundation, Merte and Clark introduced their own correlation, aligning closely with Frederking and Clark's, although with a slight alteration to

Table 3
Details concerning prior pool film boiling models and correlations.

Author(s)	Mechanism(s)	Heater Geometry	Surface Orientation	Fluid(s) considered	Comments
Bromely [31]	• Draws inspiration from Nusselt's condensation model [33]. • Noted presence of stable vapor film on lower two-thirds of the cylinder; this layer plays predominant role in facilitating majority of heat transfer from entire surface of cylinder.	Tube	Horizontal	LN_2, benzene, water, ethyl alcohol, carbon tetrachloride, n-pentane, diphenyl oxide	• Model for cylinders was modified for vertical surfaces as well.
Hsu & Westwater [49]	• Used Bromely's correlation but modified the coefficient by using their own experimental data.	Tube	Vertical	LN_2, carbon tetrachloride, methanol, benzene	• Suggested film boiling above horizontal tube should be modeled using Reynolds number.
Kutateladze [51]	• Solved equation of motion by assuming laminar flow neglecting inertial forces. • Accounted for effects of radiation.	Flat Plate	Vertical	LN_2, water, pentane, benzene, carbon tetrachloride, ethyl alcohol	• Investigated the effect of subcooling on film boiling HTC. • Showed this relationship became weaker with increasing pressure.
Chang [50]	• Analyzed film boiling by utilizing wave theory for natural convection. • Modeled liquid- vapor interface as wavey. • Introduced concept of equivalent two-phase thermal diffusivity.	Flat plate	Horizontal and vertical	Water	• Investigated effect of subcooling on film boiling HTC. • Attempted to account for radiation heat transfer. • First to consider hydrodynamic un-equilibrium effects.
Berenson [28]	• Used a concept similar to Bromley's except for incorporating utilizing the Taylor-Helmholtz hydrodynamic instability. • Combined growth rate determined from Taylor instability with geometrical and physical relations to develop HTC correlation.	Flat Plate	Horizontal	Carbon tetrachloride, n-pentane	• Accounted for effect of temperature difference on minimum heat flux
Breen & Westwater [35]	• Conducted experimental study and investigated the effect of diameter on film boiling. • They divided diameters into three categories based on ratio to Taylor most dangerous wavelength. • Observed that the HTC is independent of diameter for larger diameters for cylinders, and bubble departure is independent of diameter for small wires.	Tube and wire	Horizontal	LHe, LN_2, LH_2, LO_2, Freon 11, water, benzene, ethanol, isopropanol, n-pentane	• Confirmed validity of Bromley's correlation for intermediate diameters.
Frederking & Clark [45]	• Conducted analysis for a sphere assuming vapor layer thickness much smaller than the sphere's diameter. • Simplified their analysis by neglecting radiation, convection, and inertial effects.	Tube and Sphere	Horizontal	LN_2	• Observed that HTC is independent of heater geometry.
Merte & Clark [46]	• Used same concept as Frederking and Clark's [45] but changed the coefficient from 0.14 to 0.15.	Sphere, tube, and flat plate	Horizontal and vertical	LN_2	• They observed that heat transfer coefficient is independent of the heater geometry.
Farahat [48]	• Used integral approach by combining previous analytical and experimental works. • Observed a slip occurs at liquid-vapor interface which leads to a convection heat transfer as well.	Sphere	–	LN_2	• Correlation showed 25 % discrepancy against their experimental data.
Pomerantz [52]	• Used Bromley's correlation as basis and incorporated the wavelength along the liquid-vapor interface corresponding to the smallest unstable wave.	Tube	Horizontal	Freon 113	• Conducted hydrodynamic analysis to determine bubble frequency, spacing, and breakoff diameter.
Klimenko [42]	• Modified Berenson's model by considering including both laminar and turbulent flow within vapor film. • Adopted Reynolds' analogy. • Investigated effect of vapor film thickness and velocity on the Taylor instability. • Considered effect of friction along liquid-vapor interface.	Flat Plate	Horizontal	LN_2, LHe, LH_2, water, ethanol, Freon 113	• Correlation showed 25 % error against experimental data.
Sciance et al. [36]	Incorporated influence of reduced temperature.	Tube	Horizontal	CH_4	• Varied pressure (P_R) between 0.022 and 0.9.
Baumeister & Hamill [39, 40]	Based on concept of maximizing entropy generation within defined boundaries. Model adopts second law of thermodynamics.	Tube	Horizontal	Iso-propanol, Freon 113	• While analytical formulation showed subtle differences from Berenson's, the final correlation closely resembled Berenson's.
Sauer & Ragsdell [26]	Conducted experiments with LN_2 at atmospheric pressure and temperatures ranging from 55.56 to 611.11 K. Proposed modified form of Berenson's [28] correlation.	Flat plate	Horizontal	LN_2	• Pointed out importance of radiation effects but did not incorporated a radiation term in their HTC correlation. • Radiation effects indirectly accounted for by increasing the

(*continued on next page*)

Table 3 (*continued*)

Author(s)	Mechanism(s)	Heater Geometry	Surface Orientation	Fluid(s) considered	Comments
					coefficient of Berenson's correlation from 0.425 to 0.512.
Clements & Colver [55]	Used a concept similar to that of Sciance et al. [36]. Incorporated reduced temperature term to account for radiation effects.	Multiple geometries, including tubes, and flat surfaces	–	LN_2, LO_2, water, hydrocarbons	• Tested their correlation against over 750 datapoints and achieved a MAE of 21.8 %.
Kida et al. [56]	Conducted experiments with LN_2 over wires. Modified correlations by Bromley [31], and Breen & Westwater [35].	Wire	Horizontal	LN_2	• Determined radiation heat transfer was <20 % of total heat transfer.

the correlation's coefficient from 0.14 to 0.15. Subsequent contributions to this line of research were made by Farahat [48], who presented a similar correlation for a sphere. His modification involved changing the coefficient to 0.143 and doubling the contribution of the effective heat of vaporization, h_{fg}'. Collectively, these adjustments resulted in an overall value of the correlation's coefficient to 0.18.

$$h_{fb} = 0.143\frac{k_g}{L_x}\left[Ra_{L_x}\left(\frac{2h'_{fg}}{c_{p,g}\Delta T}\right)\right]^{0.33} = 0.18\ \frac{k_g}{L_x}\left[Ra_{L_x}\left(\frac{h'_{fg}}{c_{p,g}\Delta T}\right)\right]^{0.33} \quad (1)$$

wherein

$$Ra_{Lx} = \frac{L_x^3\ \rho_g(\rho_f - \rho_g)\ g}{\mu_g^2}\ \left(\frac{\mu_g c_{p,g}}{k_g}\right) \quad (2)$$

and L_x is the characteristic length of the film boiling system.

Over the years, there have been two important modifications to the film boiling correlations: (i) decreasing the coefficient value (e.g., from 0.62 in Bromley's correlation [31] to 0.14 in Frederking and Clark's [45]), and (ii) increasing the exponent of the Rayleigh number from 0.25 to 0.33. These refinements underscore the iterative nature of film boiling research, as scholars strive for increased predictive accuracy and applicability of their predictive models.

While acknowledging the existence of numerous additional models and correlations beyond those discussed above, this study primarily focuses on evaluating popular predictive tools rather than delving into the origins of all published tools. To ensure a comprehensive overview, the mentioned tools, alongside others, are systematically compiled and presented in Table 2, with a succinct summary of relevant information provided in Table 3.

Additionally, a compilation depicting the number of correlations is presented in Fig. 2, categorized relative to decade of publication, heater geometry, and cryogen. Notably, the data reveals that the maximum number of correlations were developed during the 1960s, for horizontal tubes, and LN_2 in particular.

In the subsequent sections of this study, the spotlight will shift to the aggregation of cryogenic data. The ensuing analysis will center on the evaluation of the aforementioned models and correlations in light of this dataset, providing a nuanced understanding of their applicability and efficacy in cryogenic scenarios.

3. New consolidated cryogenic saturated pool film boiling database

3.1. Compilation of pool film boiling data and criteria for exclusion of data points

The ongoing investigation employs a systematic methodology to collect references and data from various sources within the published literature, following a robust data mining approach similar to that recently applied by Ganesan et al. [21] for compiling cryogenic flow boiling HTC data. Primary sources for this study encompass journal articles from reputable publishers such as Springer and Elsevier, conference papers, NASA Technical Notes, and theses from global sources. The pool film boiling data was either extracted from figures in the published literature using WebPlotDigitizer [59] or from tables, where available. The data extracted from figures mostly took the form of boiling curves illustrating the different boiling regimes. Only the film boiling data are considered in this study.

Several challenges were encountered during the data mining process including (a) unavailability of certain references through Purdue University's Interlibrary Loan (ILL) services, (b) reluctance of certain investigators to share their data, and (c) instances of duplicate data. To ensure data integrity, a thorough examination was conducted to identify and eliminate duplicates. The study's primary focus on saturated pool film boiling from flat surfaces led to the intentional exclusion of data for film boiling on spheres, tubes, cylinders, wires, or narrow channels. After the initial step of eliminating duplicate data, subsequent focus was directed toward excluding additional data that did not meet the following criteria:

1. *Fluid Composition:* Only data for pure cryogenic fluids are considered; data for fluid mixtures or non-cryogenic fluids are excluded.
2. *Boiling Region:* Only pool film boiling data are considered; data for other boiling regimes are excluded.
3. *Surface Type:* Only data for pool boiling from uniformly heated flat surfaces (both 'infinite' and finite) are considered; data for tubes, wires, and spheres are excluded.
4. *Boiling State:* Only steady-state pool boiling data are considered. Excluded are sparse quench data which suffer from compromised measurement accuracy stemming from substantial and rapid variations of wall temperature during quenching experiments.
5. *Pressure and Temperature Conditions:* Only data corresponding to subcritical pressures and temperatures under saturation conditions are considered; data for supercritical conditions or subcooled liquids are excluded.
6. *Surface Orientation:* Vast majority of the available data are for horizontal and vertical surface orientations. Therefore, initial analysis is applied to these two specific orientations. However, some data are also available for the 30° and 60° orientations, which are subsequently incorporated for a comprehensive analysis of the surface orientation effects.
7. *Gravity Conditions:* Only data measured in Earth gravity are considered; data from microgravity or high gravity are excluded but will be addressed by the present authors in a future study after performing planned experiments in parabolic flight aircraft.
8. *Surface Characteristics:* Only data from smooth, micro-roughened and coated heating surfaces are considered; data from finned or greased surfaces are excluded.
9. *Data Completeness:* Only datapoints accompanied by all information essential for correlating the data, including operating pressure, heat flux, wall temperature, and surface orientation angle, are considered.

The application of these criteria resulted in a carefully curated database suitable for comprehensive analysis, as outlined in Table 4.

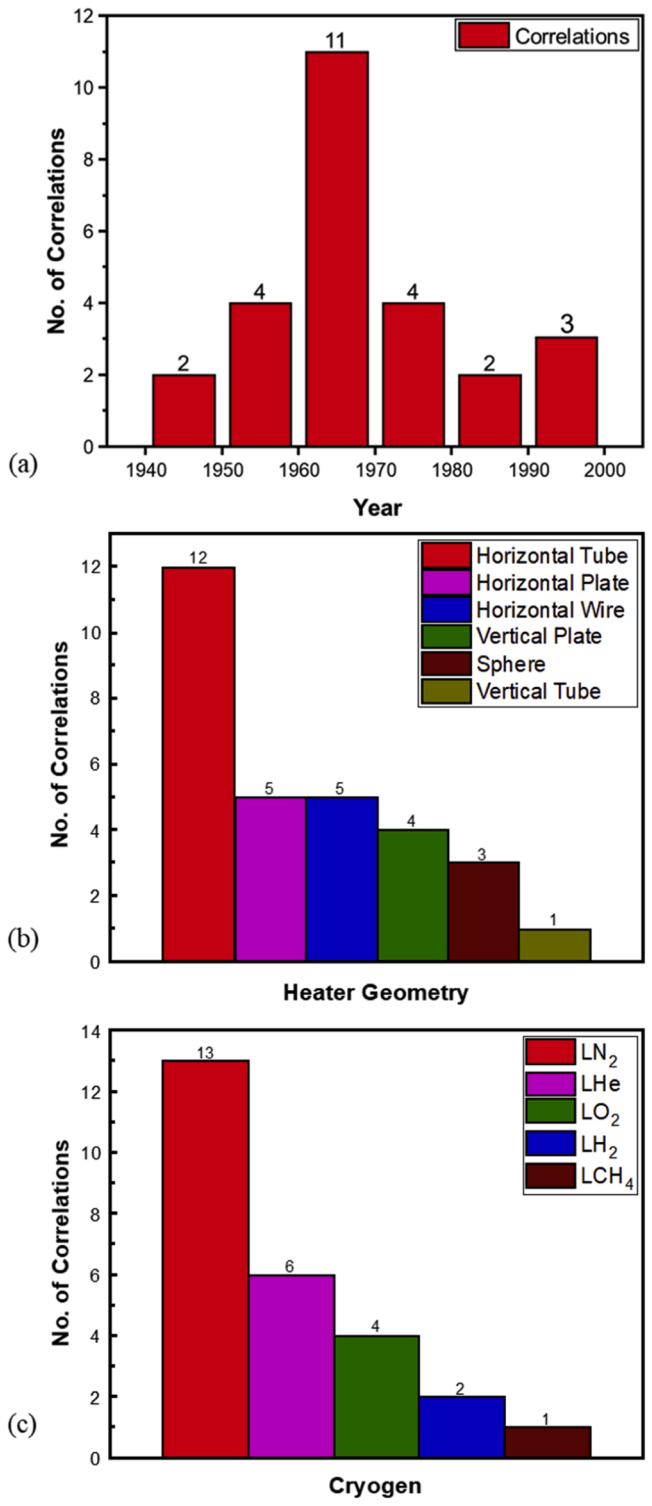

Fig. 2. Number of prior correlations and models developed (a) per decade, (b) for different heater geometries, and (c) for different cryogens.<AuQuery: Please check,Part designations in figure legends should be in normal typeface (not bold face).>

3.2. Final consolidated cryogenic pool film boiling database

The primary aim of this undertaking is to furnish the reader with a comprehensive understanding of cryogenic pool film boiling. While the specific focus of this study centers on this boiling regime, a compilation of data for other regimes has been diligently assembled to encompass the entire boiling curve. Future research articles from the Purdue University Boiling and Two-Phase Flow Laboratory (PU-BTPFL) will delve into analysis of these broader datasets. It's noteworthy that the data considered in the present study is exclusively dedicated to cryogenic saturated pool film boiling and pertains specifically to flat surfaces.

In the initial phase of the data mining (before applying the exclusion criteria), 1859 datapoints were acquired from 22 references. This dataset was subsequently categorized based on type of cryogen, as depicted in Fig. 3(a). Following this initial phase, the exclusion criteria outlined in Table 4 were meticulously applied to further refine the database. This curation process culminated in creation of the Consolidated Cryogenic Film Pool Boiling Database, abbreviated hereafter as the *Consolidated Database*. A succinct summary of the final Consolidated Database is segregated relative to cryogen, surface orientation, and decade of publication in Figs. 3(b), 3(c), and 3(d), respectively.

The ultimate iteration of the Consolidated Database encompasses a total of 1209 data points drawn from 22 references, and spans four different cryogens: LHe, LN_2, LH_2, and LAr, as detailed in Table 5. The distribution of data points across fluids is as follows: LN_2 (650), LHe (460), LH_2 (84), and LAr (15). Notably, the majority of datapoints (56.4 %) pertain to the horizontal upward-facing surface orientation ($\theta = 0°$), 27.9 % to the vertical orientation ($\theta = 90°$), 9.4 % to $\theta = 30°$, and the remaining 6.3 % to $\theta = 60°$ Excluded from the final Consolidated Database, as indicated earlier, are datapoints for subcooled, microgravity, and high gravity, which will be the subject of forthcoming studies by the authors.

3.3. Parametric distribution of consolidated database

After meticulously refining the Consolidated Database by adhering to stringent criteria, we have arrived at a comprehensive dataset comprising 1209 data points, each illuminating the nuanced behavior of cryogenic pool film boiling. This curated compilation encompasses the distinctive characteristics of four cryogenic fluids: LAr, LHe, LH_2, and LN_2, shedding light on their responses to varying system pressures, reduced pressures, HTCs, heat fluxes, wall superheats, and orientation angles.

Fig. 4 serves as a visual representation, offering insights into the distribution patterns of these crucial parameters within the Consolidated Database. The concentration of data points for LN_2 and LAr around atmospheric pressure becomes apparent, providing a foundational understanding of their behavior under typical environmental conditions. In contrast, LH_2 and LHe exhibit a more varied distribution, with data extending to higher pressures beyond the 200 kPa mark. This diversity in pressure ranges may contribute to the availability of data points capturing higher HTC values for LH_2 and LHe. Further examination reveals intriguing trends in wall superheat levels. The majority of LN_2 data is concentrated at higher wall superheat values, offering valuable insights into the behavior of this cryogen under elevated thermal conditions. Notably, there is an absence of data for LHe and LAr beyond 100 K of wall superheat, emphasizing a potential area for future exploration and experimentation. Moreover, the orientation angle analysis unveils an existing gap in data availability, particularly for surface orientations of 30° and 60° for LHe, LAr, and LH_2. This specific void points to an opportunity for future research endeavors to explore and enrich the understanding of cryogenic pool film boiling under varying orientations.

In summary, the Consolidated Database not only presents a refined and curated collection of data points but also serves as a roadmap for identifying areas where future experimental work can contribute to a more comprehensive and nuanced understanding of cryogenic pool film boiling phenomena.

3.4. Future recommendations

The parametric distribution depicted in Fig. 4, along with the earlier discussions, serves as a valuable guide in identifying critical gaps within

Table 4
Summary of total cryogenic film boiling datapoints acquired from individual sources and those excluded from consideration, along with reasons for the exclusion.

No.	Year	Author(s)	Total Acquired Datapoints	No. of Excluded Datapoints	Reasons for Data Exclusion
1	1960	Class et al. [22]	92	59	• Greased surface (13 points) • Nucleate boiling data (46 points)
2	1965	Graham et al. [60]	211	211	• Nucleate boiling data (77 points) • Unidentifiable/erroneous data (31 points) • Supercritical pressure data (62 points) • CHF data (2 points) • Hyper-g data (37 points) • Subcooled data (2 points)
3	1965	Lyon et al. [61]	198	198	• Pressure not defined (198 points)
4	1965	Wayner & Bankoff [62]	87	87	• Porous surface data (87 points)
5	1966	Cummings & Smith [63]	37	0	• No data excluded
6	1967	Clark et al. [64]	45	45	• Duplicate data from Merte [65] (45 points)
7	1969	Price [24]	338	0	• No data excluded. • This dataset include data for 30° and 60° orientations
8	1970	Merte [65]	320	275	• CHF data (15 points) • Data with pressure variations (10 points) • Natural convection data (36 points) • Transition boiling data (73 points) • Nucleate boiling data (141 points)
9	1972	Sauer & Ragsdell [26]	61	0	• No data excluded
10	1977	Deev et al. [66]	159	102	• Nucleate boiling data (102 points)
11	1977	Grigoriev et al. [67]	41	8	• Non-stationary data (8 points)
12	1981	Ogata et al. [68]	54	39	• Nucleate boiling data (24 points) • Grooved surfaces data (15)
13	1982	Kleminko & Shelepen [69]	75	0	• No data excluded
14	1982	Schiewe & Hartmann [70]	79	0	• No data excluded
15	1986	Nishio [71]	425	425	• Unsteady data (318 points) • Transition boiling data (86 points) • Transient data (11 points) • Nucleate boiling data (10 points)
16	1989	Chandratilleke et al. [72]	252	175	• Nucleate boiling data (65 points)
17	1989	Nishio & Chandratilleke [73]	122	92	• Nucleate boiling data (92 points)
18	1992	Kozlov & Nozdrin [74]	68	40	• Nucleate boiling data (35 points) • CHF data (5 points)
19	1993	Ogata & Mori [75]	122	76	• Transition boiling data (76 points)
20	1998	Iwamoto et al. [76]	259	130	• Nucleate boiling data (129 points)
21	2009	Jin et al. [77]	180	83	• Natural convection data (15 points) • Nucleate boiling data (29 points) • Transition boiling data (39 points)
22	2015	Balakin et al. [78]	193	166	• Natural convection data (45 points) • Nucleate boiling data (121 points)

the available cryogenic data. Based on these insights, the following recommendations are proposed for future experimental work:

i. Historically, researchers have predominantly focused on geometries like tubes, wires, and spheres. Future studies should emphasize investigating and collecting data specifically for flat plate surfaces to enhance the understanding of cryogenic pool film boiling for this geometry.
ii. While there is a substantial amount of data available for LN_2 and LHe, there is a noticeable scarcity of data for cryogens such as LAr and LH_2. Additionally, no usable data is available for LO_2, LCH_4, or parahydrogen. Future experimental efforts should prioritize collecting data for these less-explored cryogens to achieve a more comprehensive understanding of their cryogenic pool film boiling characteristics.
iii. The existing data for the horizontal orientation is relatively sufficient; however, there is a clear need for additional experiments to cover other orientations. Future studies should aim to provide a more balanced dataset across various surface orientations to capture the full spectrum of boiling behaviors in film boiling regime.
iv. While LN_2 has been extensively studied, there is a need for future experiments to explore elevated pressures, temperatures, and high heat fluxes for all cryogens. This will contribute to a more comprehensive and diverse dataset, allowing for a deeper understanding of cryogenic pool film boiling across a wider range of operating conditions.

In summary, future experimental endeavors should prioritize providing comprehensive information for correlating data. This includes documenting crucial parameters such as pressure, heat flux, wall temperature, HTC, heating wall properties (material, thermal properties, size, shape, and thickness), and, importantly, surface orientation. Addressing these recommendations will contribute to bridging existing gaps in cryogenic data and advancing the understanding of pool film boiling phenomena for various cryogens and surface geometries.

4. Assessment of prior models and correlations

Following an exhaustive literature review, a comprehensive compilation of 23 distinct models and correlations has been assembled, as detailed in Table 2. Given the analogous structure of these correlations and their shared evaluative criteria, categorization into sub-groups based on any discernible basis proves challenging. The uniformity in form and the common thread of evaluation underscores the need for a collective and unbiased assessment of these diverse models.

4.1. Statistical parameters and methodology for assessment

The utilization of the Consolidated Database serves as a pivotal step in the evaluation of the predictive accuracy exhibited by all the scrutinized models and correlations in forecasting the film boiling heat transfer coefficient (HTC). This comprehensive assessment involves the application of three distinct statistical parameters: mean absolute error (MAE), percentage of datapoints predicted within ±30 % of experiment

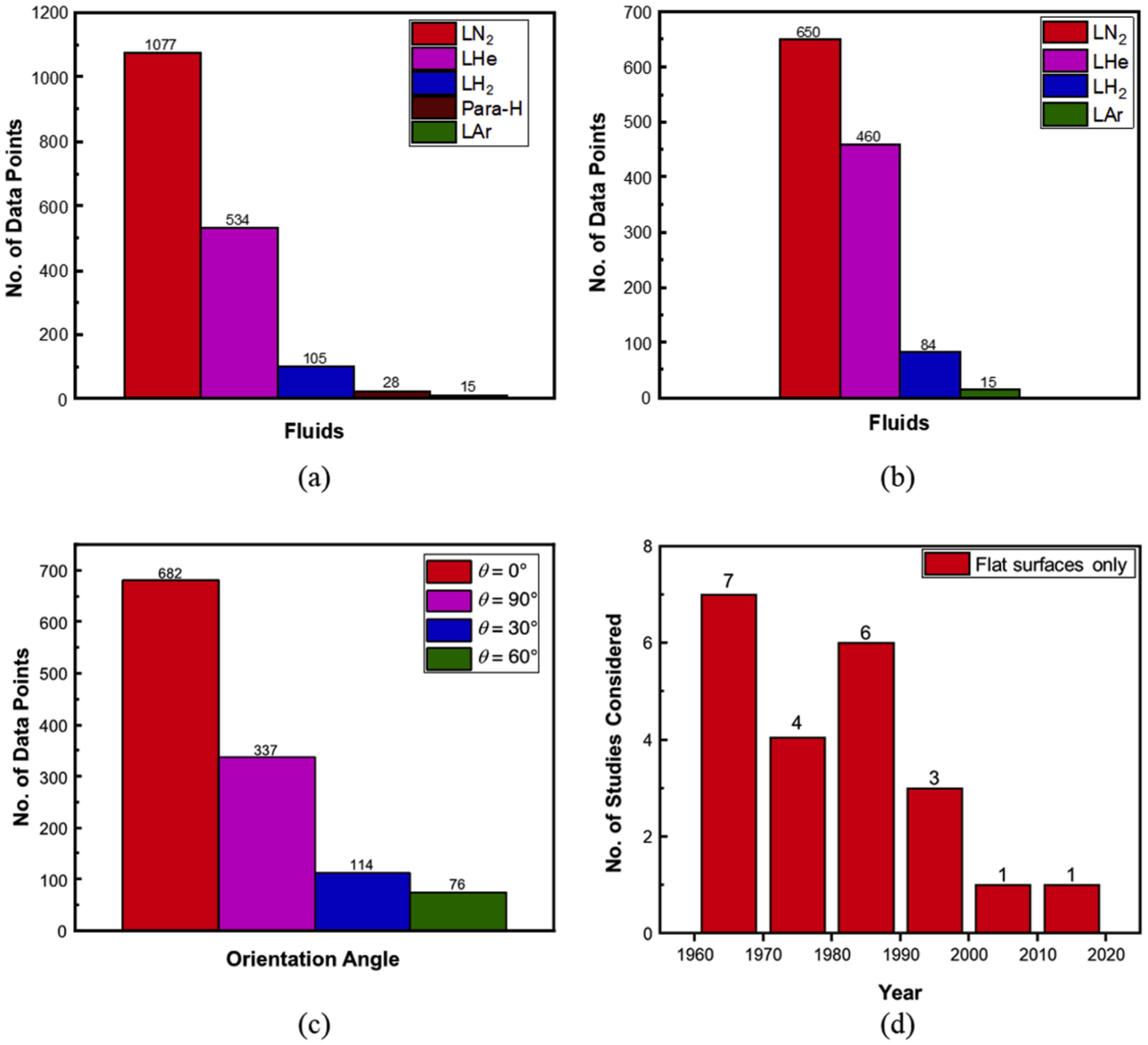

Fig. 3. Summary of database (a) before applying exclusion criteria and (b) after applying exclusion criteria (Consolidated Database). Segregation of Consolidated Database relative to (c) orientation angle and (d) decade of publication.

(α), and the percentage of datapoints predicted within ±50 % (β). To furnish thermophysical properties essential for this evaluation, REFPROP 10 [20] is employed, offering a comprehensive representation of fluid characteristics across diverse pressures and temperatures.

The mean absolute error (MAE), a fundamental metric in this analysis, is defined as the average absolute difference between the predicted HTC value derived from a correlation or model and the corresponding experimental value included in the Consolidated Database.

$$MAE = \frac{1}{N}\sum \frac{|HTC_{Pred} - HTC_{Exp}|}{HTC_{Exp}} \times 100\% \quad (3)$$

where N is the number of datapoints. By employing these diverse statistical parameters, the assessment process strives to offer a robust and nuanced understanding of the predictive capabilities inherent in the reviewed models and correlations. This multifaceted analysis aims to transcend mere numerical accuracy, providing a comprehensive insight into the reliability and efficacy of the predictive models across various conditions and scenarios within the realm of film boiling.

4.2. Assessment and comparison of prior predictive tools

The influence of surface orientation in film boiling assumes a pivotal role, given the disparities in the underlying fluid physics between various orientations, most notably horizontal and vertical. Consequently, the study systematically compares results for different orientations using distinct graphs, aligning with established literature practices where authors segregate data based on orientation. Given the primary focus of the present investigation on horizontal and vertical orientations, the subsequent sections will specifically delve into the comparison of previously established predictive tools for data in these two orientations. However, it's worth noting that data pertaining to other orientations (30° and 60°) will be presented in a subsequent section; however, exclusively focusing on the best correlations identified in the study. This structured approach ensures a thorough examination of film boiling characteristics across different orientations while maintaining clarity and focus on the comparative analysis.

It is noteworthy to highlight that a substantial proportion of prior predictive tools is not specifically formulated for flat plate horizontal and vertical orientations, thus underscoring one of the primary

Table 5
Summary of Consolidated Database.

Reference	Acceptable Datapoints	Heater Geometry	Heater Size: Width x Length [mm^2] or Diameter (Thickness) [mm]	Heater Material	Surface roughness [μm]	Pressure [MPa]	Inclination Angle	Boiling State
LN_2								
Price (1969) [24]	338	Rectangular	50.8 × 101.6	Inconel 600	Mirror finish	0.10133	0°, 30°, 60°, 90°	Saturated
Sauer & Ragsdell (1972) [26]	61	Rectangular	12.7 × 101.6, 25.4 × 101.6, 50.8 × 101.6	Inconel 600	Mirror finish	0.10133	0°	Saturated
Merte (1970) [65]	22	Circular	76.2 (20.64)	Copper	600 grit	0.0986	0°, 90°	Saturated
Kleminko & Shelepen (1982) [69]	26	Disk	40 (20)	Copper	Not mentioned	0.10133	0°	Saturated
Schiewe & Hartmann (1982) [70]	79	Rectangular	–	Copper	0.75 12.6	0.10133	0°	Saturated
Jin et al. (2009) [77]	97	Square	60 × 60 (17.5)	Stainless steel	Not mentioned	0.1	0°	Saturated
Balakin et al. (2015) [78]	27	Rectangular	(25–40) x 2.5, (0.08)	Ni – W tape	Not mentioned	0.1013	0°, 90°	Saturated
	650	***Total acceptable datapoints for LN_2***						
LHe								
Cummings & Smith [65]	37	Circular	15.24	Copper	240 grit	0.10133	0°	Saturated
Grigoriev et al. (1977) [67]	34	Circular	8	Copper M-1, stainless steel X18H9T	7	0.10133	0°	Saturated
Deev et al. (1977) [66]	57	Square	30 × 30	Copper (99.993 %)	0.1	0.1 – 0.223	0°	Saturated
Ogata et al. (1981) [68]	15	Square	15 × 15	Copper	Smooth; oxidized smooth	0.10133	0°	Saturated
Kleminko & Shelepen (1982) [69]	34	Disk	40 (20)	Copper	Not mentioned	0.10133	0°	Saturated
Chandratilleke et al. (1989) [72]	77	Circular	20 (30)	Copper	smooth	0.10133	0°, 90°	Saturated
Nishio & Chandratilleke (1989) [73]	30	Circular	20 (30)	Copper	smooth	0.10133	90°	Saturated
Ogata et al. (1993) [75]	46	Square	15 × 15 (8)	Copper	Smooth	0.10133	0°, 90°	Saturated
Iwamoto et al. (1998) [76]	130	Rectangular	18 × 10 (7.5), 18 × 18 (7.5), 18 × 40 (7.5), 18 × 76 (7.5)	Copper	Polished (roughness below 10 μm)	0.1013	0°, 90°	Saturated
	460	***Acceptable LHe datapoints***						
LH_2								
Class et al. (1960) [22]	33	Rectangular	25.4 × 558.8 (0.127)	Karma alloy	0.13729 μm	0.10133 – 0.88153	0°, 90°	Saturated
Merte (1970) [65]	23	Circular	76.2	Copper	600 grit	0.1023 – 0.1027	0°, 90°	Saturated
Kozlov & Nozdrin (1992) [74]	28	Circular	30 (8, 18, 12)	Stainless steel, aluminum alloy, copper	Not mentioned	0.016 – 0.13	0°	Saturated
	84	***Acceptable LH_2 datapoints***						
LAr								
Kleminko & Shelepen (1982) [69]	15	Disk	40 (20)	Copper	Not mentioned	0.10133	0°	Saturated
	15	***Acceptable LAr datapoints***						
	1209	***Total acceptable data points for all four cryogens***						

motivations behind this study. Despite this, a meticulous evaluation of all predictive tools is undertaken simultaneously for all data points in the Consolidated Database. This approach is grounded in two compelling reasons. Firstly, as previously mentioned, there exists a perspective among some authors asserting that the correlation for film boiling HTC is independent of heater geometry. Secondly, this comprehensive evaluation is aimed at scrutinizing the entirety of prior correlations, laying the groundwork for development of a new correlation that could outperform its predecessors. This dual-pronged rationale ensures a thorough exploration of the existing tools while concurrently paving the way for potential advancements in the understanding and prediction of film boiling HTC.

4.2.1. Comparison of prior tools against horizontal orientation data

Over the past few decades, the focus on flat surfaces has been relatively overshadowed by research on wires and tubes. Nevertheless, horizontal flat surfaces have garnered a notable level of interest, making data acquisition for the horizontal orientation reasonably accessible. The Consolidated Database encompasses 682 data points specifically curated for horizontal orientation, serving as a comprehensive dataset to rigorously test prior predictive tools. The large number of prior tools makes it practically unfeasible to compare all of them in a single

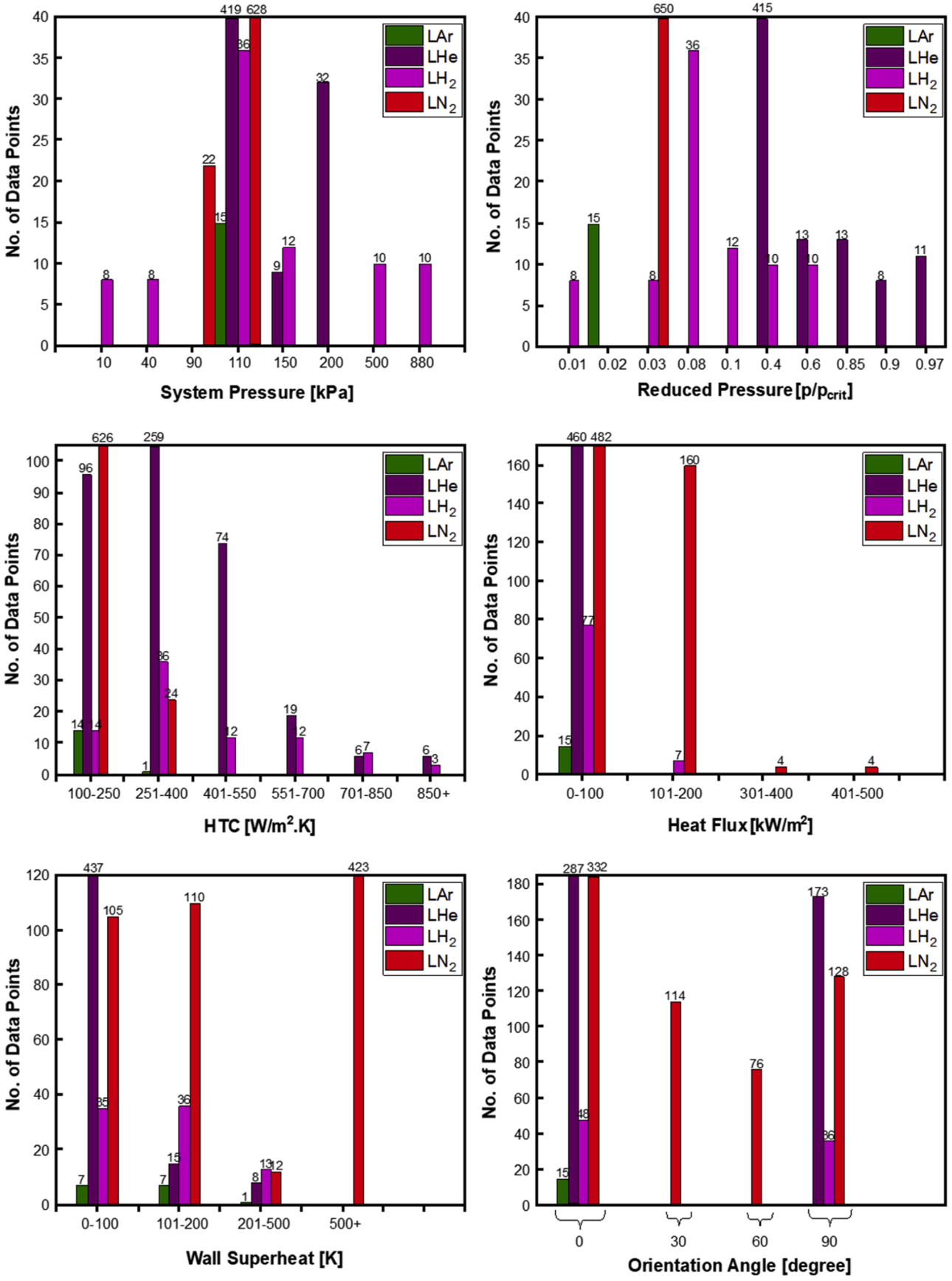

Fig. 4. Parametric distribution of Consolidated Database.

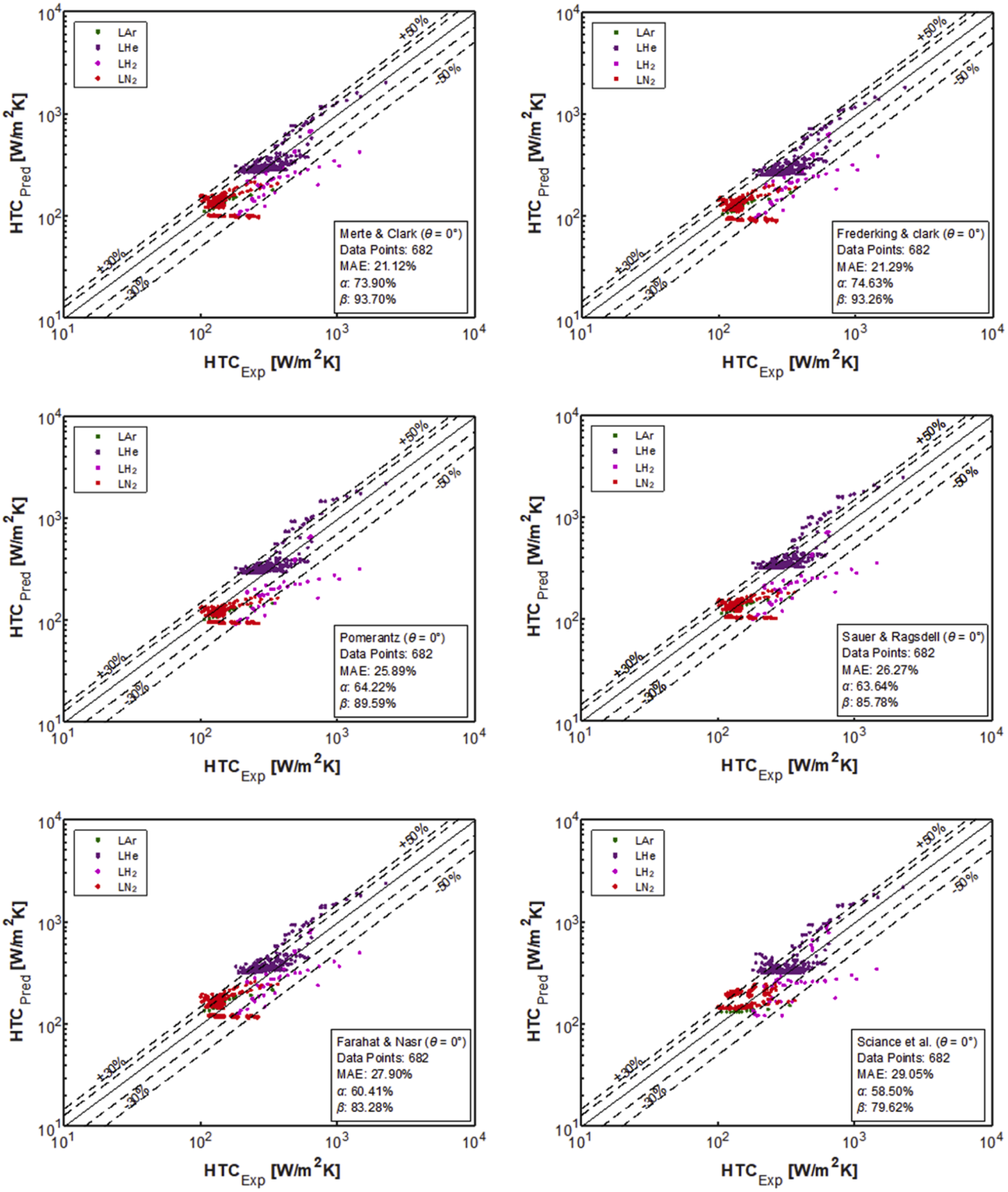

Fig. 5. Comparison of prior correlations giving best performance for film boiling on flat horizontal surface.

visualization. Consequently, to facilitate a more trackable analysis, these prior tools are categorized into three groups based on their MAEs. This strategic grouping allows for a nuanced examination of the performance of different tools within distinct error ranges, contributing to a more insightful and efficient assessment process.

In Fig. 5, the comparison of the first category is presented exclusively for the horizontal orientation and six prior tools having a MAE below 30 %, designating them as the top-performing prior correlations and models for pool film boiling from horizontal surfaces. Merte and Clark [46] emerge as the standout performers with a remarkable 21.12 % MAE, closely followed by Frederking and Clark [45] with a similarly impressive 21.29 % MAE. The striking similarity in performance between these two correlations is attributed to their nearly identical formulations, differing only in minimal coefficient adjustments ($C_1 = 0.14$ in Frederking and Clark versus 0.15 in Merte and Clark). It is noteworthy that these correlations were originally developed for film boiling over a

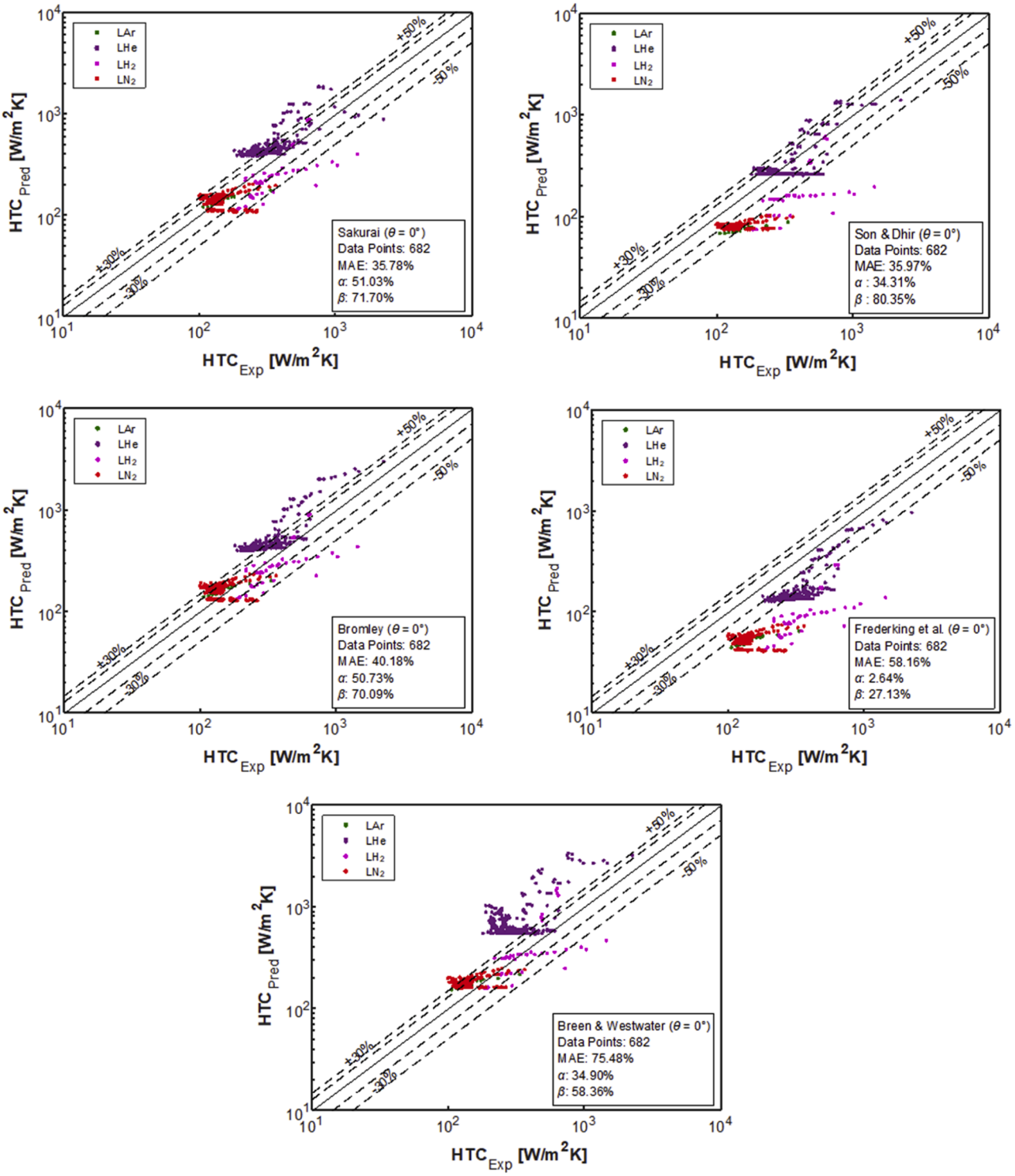

Fig. 6. Comparison of prior correlations giving medium performance for film boiling on flat horizontal surface.

spherical body but exhibit excellent performance for horizontal flat surfaces as well. Following the exemplary works of Merte and Clark and Frederking and Clark, the correlations by Pomerantz [52], Sauer and Ragsdell [26], Farahat and Nasr [48], and Sciance et al. [36] also demonstrate commendable performance, evidenced by MAEs of 25.89 %, 26.27 %, 27.9 %, and 29.05 %, respectively.

Moving on to the second category, which encompasses five correlations, the performance of which is illustrated in Fig. 6. These correlations exhibit MAEs ranging from 35 % to 76 %, categorizing them as moderately performing correlations for film boiling over horizontal flat surfaces. This category includes Sakurai [37], Son and Dhir [58], Bromley [31], Frederking et al. [41], and Breen and Westwater [35], with corresponding MAEs of 35.78 %, 35.97 %, 40.18 %, 58.16 %, and 75.48 %, respectively.

Lastly, a third category comprises five correlations whose performance is depicted in Fig. 7, where the MAEs exceed 100 %. These correlations consistently overpredict the performance of film boiling over horizontal flat surfaces and are deemed not recommended for this

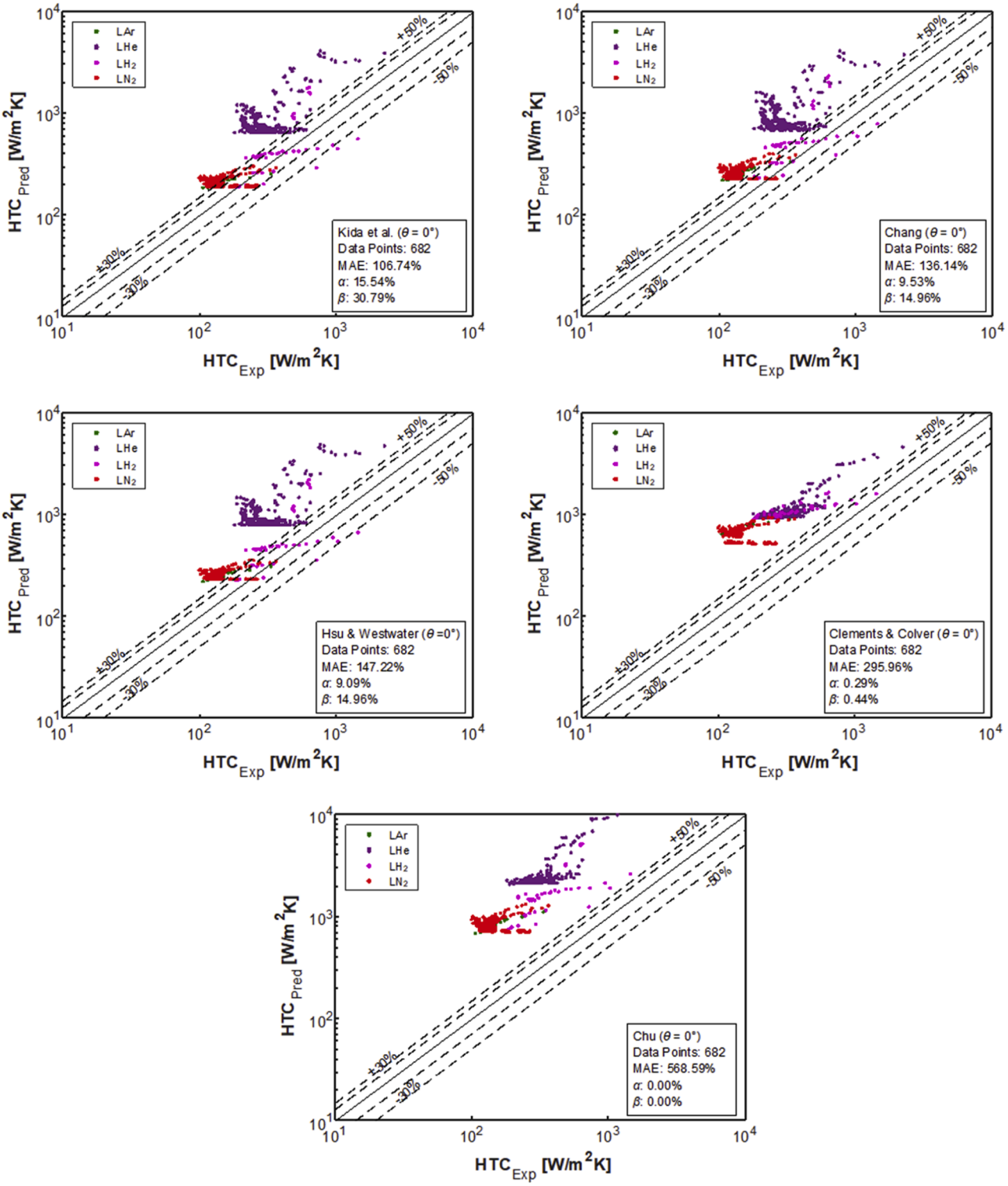

Fig. 7. Comparison of prior correlations giving worst performance for film boiling on flat horizontal surface.

configuration. The correlations in this category include Kida et al. [56], Chang [29], Hsu and Westwater [49], Clements and Colver [55], and Chu [57], with corresponding MAEs of 106.74 %, 136.14 %, 147.22 %, 295.96 %, and 568.59 %, respectively. This classification provides a comprehensive breakdown of the performance of prior predictive tools, aiding in the selection of appropriate formulations for assessing film boiling over horizontal flat surfaces.

4.2.2. *Comparison of prior tools against vertical orientation data*

In contrast to film boiling over horizontal surfaces, the vertical orientation has received comparatively less attention from researchers, resulting in limited available data for this orientation. Nevertheless, there is sufficient data to evaluate prior correlations and offer insights for the development of an improved correlation. The Consolidated Database in this study encompasses 337 data points specifically curated for vertical orientation. It's worth noting that no data was available for LAr in vertical orientation. Similar to the categorization for horizontal

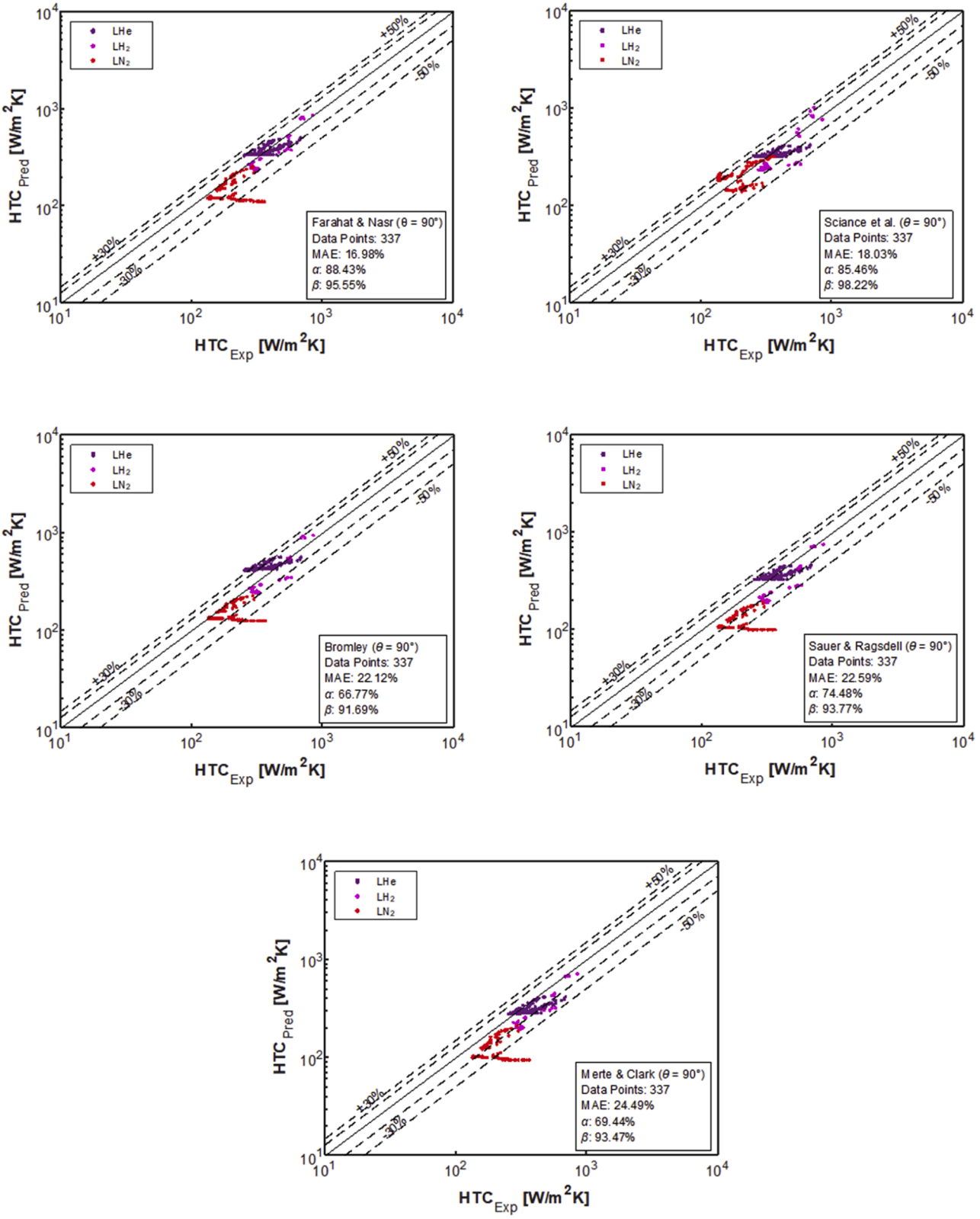

Fig. 8. Comparison of prior correlations giving best performance for film boiling on flat vertical surface.

orientations, the correlations for vertical orientations are also divided into three categories based on their MAEs for ease of presentation. However, this categorization differs from the previous one as these correlations perform differently for various orientations.

The comparison of the first category of correlations for flat plate vertical surfaces is depicted in Fig. 8. This category, comprising five correlations, demonstrates remarkable performance, with all MAEs falling below 25 %. Notably, the correlations of Farahat and Nasr [48] and Sciance et al. [36] stand out, achieving MAEs of 16.98 % and 18.03 %, respectively, and establishing themselves as top-performing

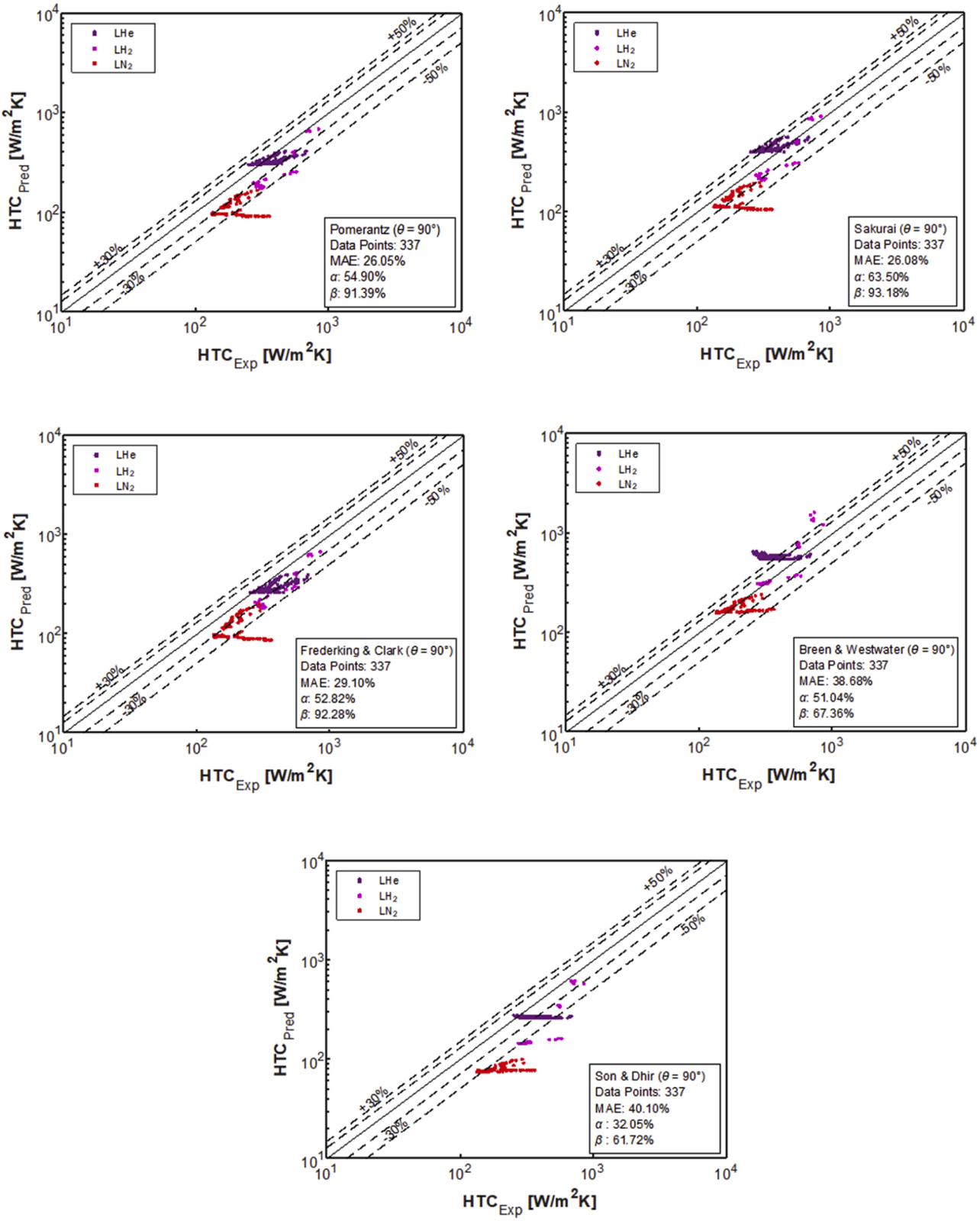

Fig. 9. Comparison of prior correlations giving medium performance for film boiling on flat vertical surface.

predictive tools for the vertical orientation. Following closely, the correlations of Bromley [31], Sauer and Ragsdell [26], and Merte and Clark [46] also perform exceptionally well, attaining respective MAEs of 22.12 %, 22.59 %, and 24.49 %. Collectively, these correlations are considered as the best for film boiling over flat plate vertical surfaces.

Moving on to the second category, encompassing five correlations, the performance is illustrated in Fig. 9. These correlations exhibit MAEs ranging from 25 % to 40 %, categorizing them as moderately performing correlations for film boiling over vertical flat surfaces. This category includes the correlations of Pomerantz [52], Sakurai [37], Frederking

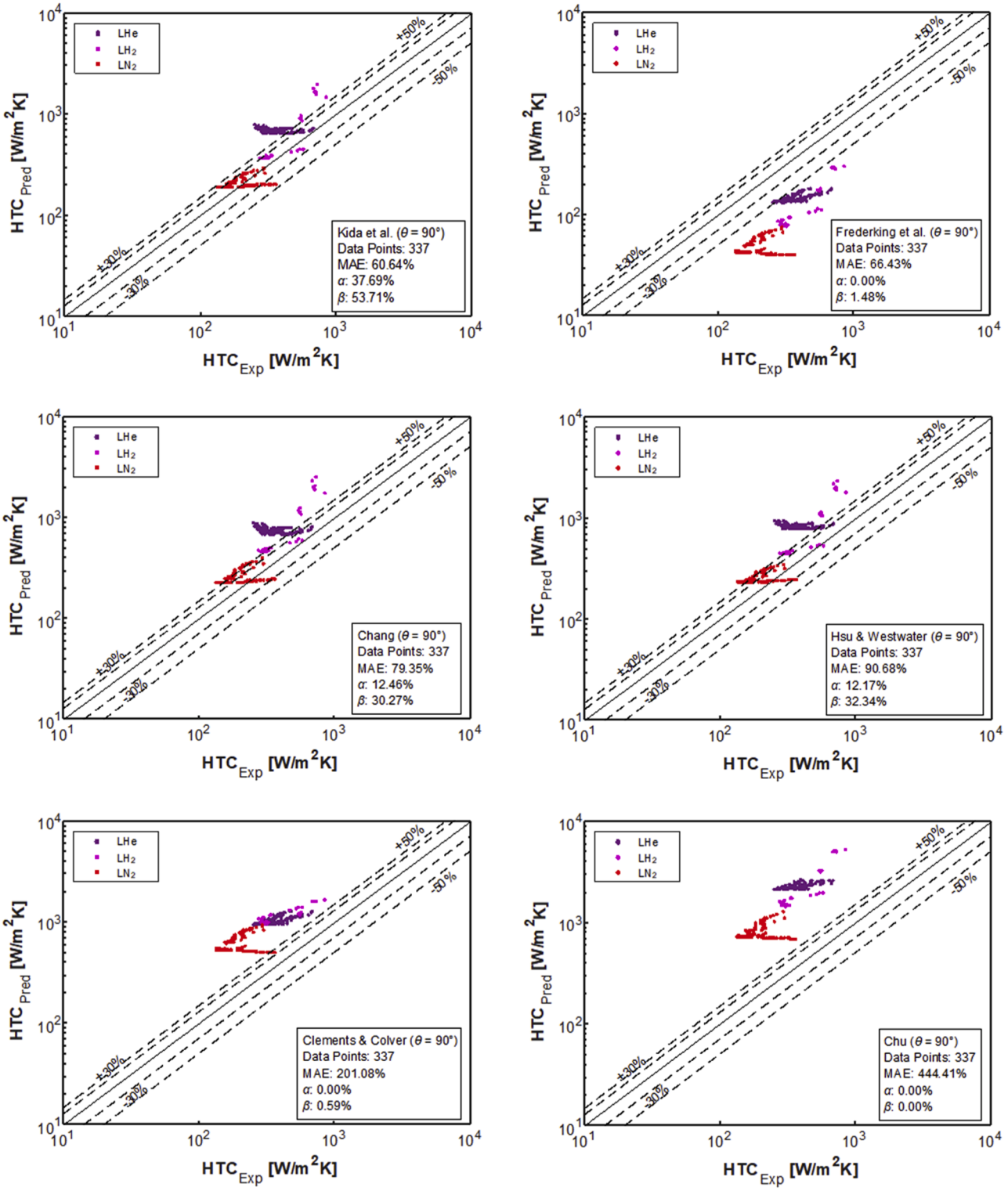

Fig. 10. Comparison of prior correlations giving worst performance for film boiling on flat vertical surface.

and Clark[45], Breen and Westwater [35], and Son and Dhir [58], with their corresponding MAEs of 26.05 %, 26.08 %, 29.10 %, 38.68 %, and 40.10 %, respectively. Notably, the correlations of Merte and Clark [46] and Frederking and Clark [45] exhibit distinct performances in this case compared to the horizontal orientation, emphasizing the prominent effect of coefficients in vertical orientation, demanding a careful consideration in their selection.

Lastly, the third category comprises six correlations, as shown in Fig. 10. The MAEs of the first four are <100 %, categorizing them as mediocre, while the last two exceed 100 %, indicating consistently overpredicted performance. Given the availability of superior correlations for vertical orientations, this last category is not recommended for assessing film boiling performance over vertical surfaces. The correlations in this category include Kida et al. [56], Frederking et al. [41], Chang [29], Hsu and Westwater [49], Clements and Colver [55], and Chu [57], with corresponding MAEs of 60.64 %, 66.43 %, 79.35 %,

90.68 %, 201.08 %, and 444.41 %, respectively.

5. New universal saturated pool film boiling correlation

5.1. Development of new universal correlation for cryogenic pool film boiling

The process of developing a new correlation for pool film boiling involved a meticulous analysis of existing experimental data and a sincere acknowledgment of the contributions made by previous researchers in this field. Recognizing the collaborative nature of scientific endeavors and the ongoing pursuit of improvement, this study aims to build upon the foundations laid by earlier authors in the realm of pool film boiling. A comprehensive examination of the experimental data underscored the need to critically evaluate existing correlations. Embracing the ethos of continual improvement, this study positions itself as a proactive effort to enhance the body of knowledge established by predecessors.

Upon close scrutiny, a discernible pattern emerged, revealing that the majority of prior correlations for pool film boiling HTC could be encapsulated within a general mathematical form given by Eq. (3). This observation underscores the interconnectedness of research efforts and the iterative nature of scientific progress.

$$h_{fb} = \frac{k_g}{L_x} C_1 \left[Ra_{L_x} \left(\frac{h'_{fg}}{c_{p,g} \Delta T} \right) \right]^m \tag{4}$$

where h_{fb} is the film boiling HTC, Ra_{Lx} is the Rayleigh number based on characteristic length L_x, which is equal to L_b for flat plate surfaces, C_1 is the coefficient of correlation, m is the exponent, and the term h_{fg}' represents the modified heat of vaporization, which accounts for both sensible and latent heat transfer, and is given by:

$$h'_{fg} = h_{fg} + A\ c_{p,g}\ \Delta T \tag{5}$$

where $\Delta T = T_w - T_{sat}$ for saturated pool film boiling and A is an empirical coefficient. Upon careful examination of existing correlations, researchers have consistently sought to enhance the HTC correlation by refining the values of C_1 and m. The consensus among most authors is that the exponent m falls within the range of 0.25 to 0.33, while C_1 varies between 0.14 and 0.667. The coefficient A has predominantly remained at 0.5 in most correlations. Notably, a shift has occurred over time, with earlier authors favoring lower values of m and higher values of C_1, while recent research tends to adopt the inverse trend. Evaluating correlations based on flat surface geometries, it becomes apparent that these surfaces tend to favor lower C_1 values and higher m values, aligning with the latest research trends.

Given the consistent disparity between horizontal and vertical orientation data, a closer examination was conducted to identify favorable values for C_1, m, and A for individual orientations. It was found that a preferred value for m across all orientations is 0.33, and for A, it is 0.46. The preferred range for C_1 varied between 0.148 and 0.2 for different orientations from horizontal to vertical. Remarkably, this trend exhibited monotonicity across all orientations, facilitating the generalization of the new correlation. These values were finalized based on insights from prior correlations and a regression analysis conducted using a custom Python program.

After optimizing the coefficients and exponents in Eqs. (3) and (4), the results were compared with prior correlations, revealing that the new correlation achieved the lowest MAE among all previous correlations. However, upon further examination of the Consolidated Database, it became apparent that all correlations, including the new one, consistently underestimated HTC for data points at elevated temperatures. This prompted a reconsideration of the inclusion of a radiation term in the new correlation.

Before proceeding, it was essential to illustrate the sole effect of radiation heat transfer with respect to temperature. The radiation HTC was calculated using the following equation:

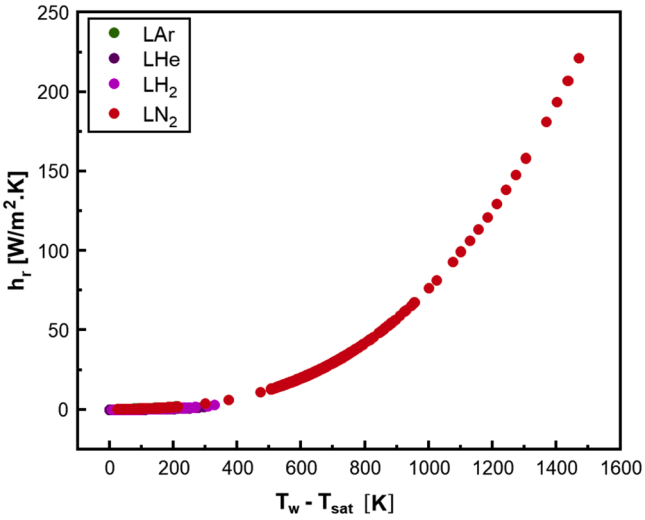

Fig. 11. Variation of radiation heat transfer coefficient with wall superheat.

$$h_r = B(\varepsilon)\ \sigma_b\ \frac{\left(T_w^4 - T_{sat}^4\right)}{\left(T_w - T_{sat}\right)} \tag{6}$$

where ε and σ_b are, respectively, the surface emissivity and the Stefan-Boltzmann constant (5.67×10^{-8} W/m^2.K^4). The above equation introduces the function B, representing a correlation coefficient for radiation heat transfer that is derived through regression analysis. Determining the radiation HTC presents a significant challenge due to the complex dependence of emissivity on various factors such as temperature, heated surface material, and roughness. To simplify this, the surface temperature and surface property effects on emissivity are lumped into the coefficient B. Results based on temperature conditions from the Consolidated Database are depicted in Fig. 11. The graphical representation in Fig. 11 highlights the increasing importance of the radiation heat transfer term at elevated temperatures, particularly above 500 K. This observation aligns with findings in the literature, as discussed in Section 1.5.

Subsequently, Eq. (6) was combined with Eqs. (4) and (5). The coefficient B was fine-tuned for different orientations to achieve the most accurate correlation. After incorporating all the necessary terms and adjustments discussed, the final correlation for pool film boiling emerged as follows:

$$h_{fb} = (0.148 + 0.052\ sin\theta)\ \frac{k_g}{L_x}\left[Ra_{Lx} \cdot \left(\frac{h_{fg} + 0.46\ c_{p,g}\ (T_w - T_{sat})}{c_{p,g}\ (T_w - T_{sat})} \right) \right]^{0.33} + \frac{(1.7 - 0.55\ sin\theta)\ \sigma_b\ \left(T_w^4 - T_{sat}^4\right)}{(T_w - T_{sat})} \tag{7}$$

where h_{fb} is the *overall* film boiling HTC [W/m^2.K], θ is the orientation angle of the heated surface measured from horizontal upward position [degrees], h_{fg} is the latent heat of vaporization [J/kg], $c_{p,g}$ is the specific heat of saturated vapor at constant pressure [J/kg.K], T_w is the temperature of the heated wall [K], T_{sat} is the saturation temperature of the liquid pool at the given pressure [K], and L_x is the characteristic length [m] which, for the case of flat surfaces, is equal to the bubble length scale (L_b), defined as

$$L_b = \left[\frac{\sigma}{g(\rho_f - \rho_g)} \right]^{\frac{1}{2}} \tag{8}$$

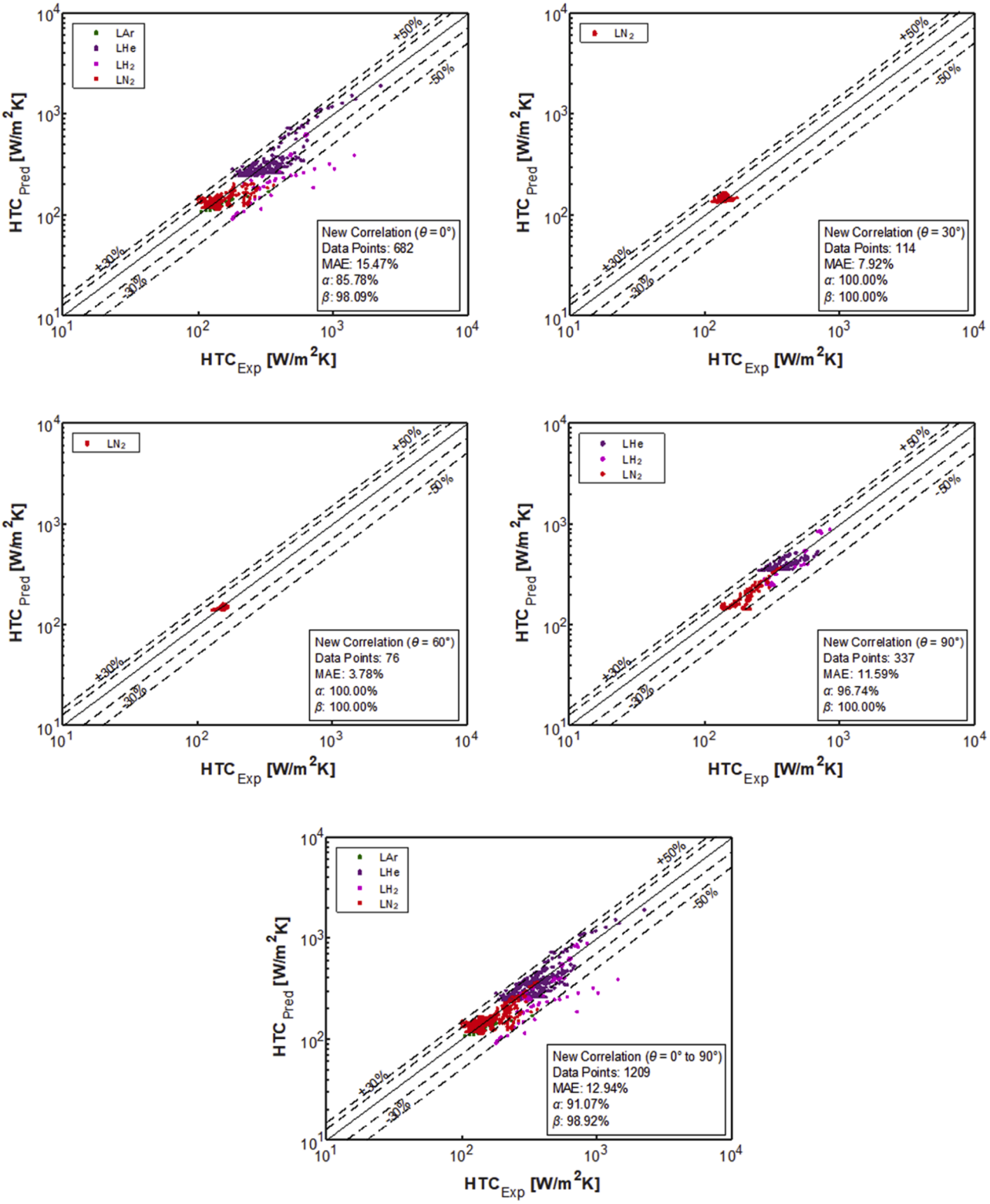

Fig. 12. Assessment of the new correlation against the Consolidated Database for 0°, 30°, 60°, 90°, and combined orientations.

Ra_{Lx} in Eq. (7) is the Rayleigh number which is defined in Eq. (2) wherein ρ_g, ρ_f, μ_g, and k_g are the density of saturated vapor [kg.m^{-3}], density of saturated liquid [kg.m^{-3}], viscosity of saturated vapor [Pa.s] and thermal conductivity of saturated vapor [W.m^{-1}.K^{-1}], respectively, all of which being based on the given saturation pressure of fluid.

The predictions of the new correlation are presented in Fig. 12, showcasing its performance across various surface orientation angles, including horizontal (θ = 0°), vertical (90°), 30°, and 60°, as well as combined range from horizontal to vertical. The new correlation exhibits a remarkable MAE of 15.47 % for horizontal orientation, with 85.78 % and 98.09 % of predictions falling within ±30 % (α) and ±50 % (β) of the data, respectively. For vertical orientation, the MAE is even lower at 11.59 %, accompanied by 96.74 % and 100 % of predictions within ±30 % and ±50 % of the data, respectively. Furthermore, the

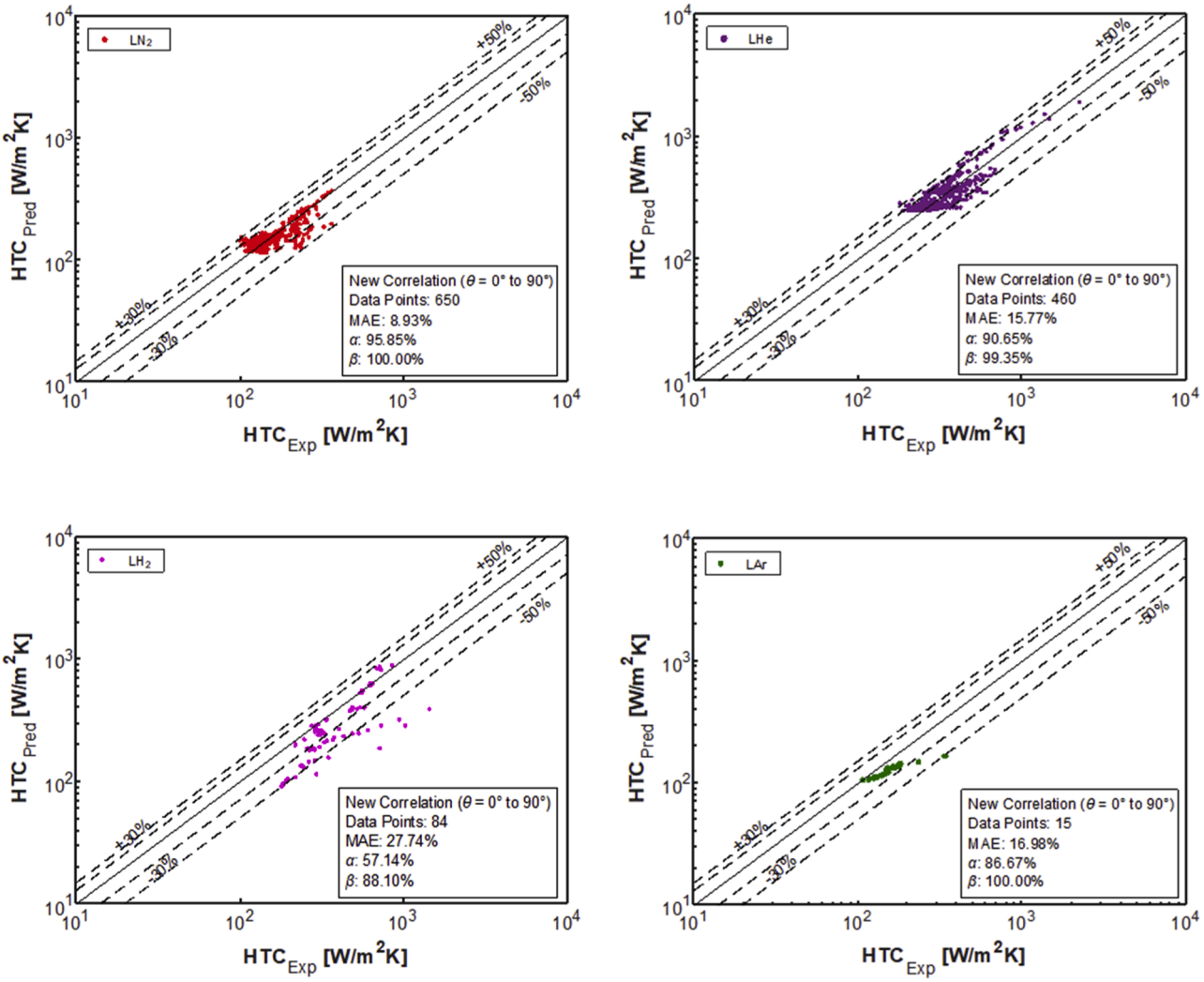

Fig. 13. Assessment of the new correlation against the Consolidated Database for individual cryogens and all orientations from 0° to 90°

new correlation underwent testing with limited available data for orientations $\theta = 30°$ and $\theta = 60°$ Impressively, it achieved an MAE of 7.92 % for $\theta = 30°$, with 100 % of predictions within both ±30 % and ±50 % of the data. Similarly, for $\theta = 60°$, the new correlation attained an MAE of 3.78 %, with a perfect 100 % of predictions falling within both ±30 % and ±50 % of the data.

In an overarching assessment, combining data from all orientations (0° to 90°), the new correlation outperformed all prior correlations, securing an overall MAE of 12.94 %. Notably, 91.07 % and 98.92 % of predictions are within ±30 % and ±50 % of the data, respectively. It is important to highlight that the performance of the new correlation exhibited an upward trend with increasing surface orientation angle. This suggests that the new correlation may offer promising accuracy for orientation angles beyond 90°, excepting angles near 180° due to the distinct fluid physics differences between horizontal upward and horizontal downward orientations. Future researchers are encouraged to explore and validate the new correlation for additional angles, making adjustments as necessary based on observed performance.

While the new correlation demonstrates exceptional overall performance across diverse cryogens, a thorough evaluation for each cryogen individually provides valuable insights. The independent performance of the new correlation for each cryogen is illustrated in Fig. 13. The new correlation excels when applied to LN_2, achieving an impressive MAE of 8.93 %, with 95.85 % of predictions within ±30 % and a perfect 100 % within ±50 %. Following closely, LHe also shows strong performance with a MAE of 15.77 %, α of 90.65 %, and β of 99.35 %. LAr, while exhibiting a slightly higher MAE of 16.98 %, maintains robust performance with 86.67 % within ±30 % and 100 % within ±50 %. LH_2, while presenting a higher MAE of 27.74 %, still demonstrates satisfactory results, with 57.14 % within ±30 % and 88.10 % within ±50 %. The designation of the new correlation as a *universal correlation* is rooted in its consistent and reliable performance across different cryogenic fluids.

5.2. Comparison of new correlation with best prior correlations for horizontal and vertical orientations

The comprehensive evaluation of the new correlation's performance involves a comparative analysis with the three best prior correlations for both horizontal and vertical orientations. This comparison aims to highlight the effectiveness of the new correlation in achieving lower MAE values compared to its counterparts.

For horizontal orientation, comparing the performance of the new correlation from Fig. 12 to those in Fig. 5 for best performing prior correlations shows obvious superiority of the new correlation, evidence by a MAE of 15.47 % compared to MAE values for Merte and Clark [46], Frederking and Clark [45], and Pomerantz [52] of 21.12 %, 21.29 %, and 25.89 %, respectively.

Similarly, for vertical orientation, comparing the performance of the new correlation from Fig. 12 to those in Fig. 8 for best performing prior correlations shows additional proof of superiority of the new

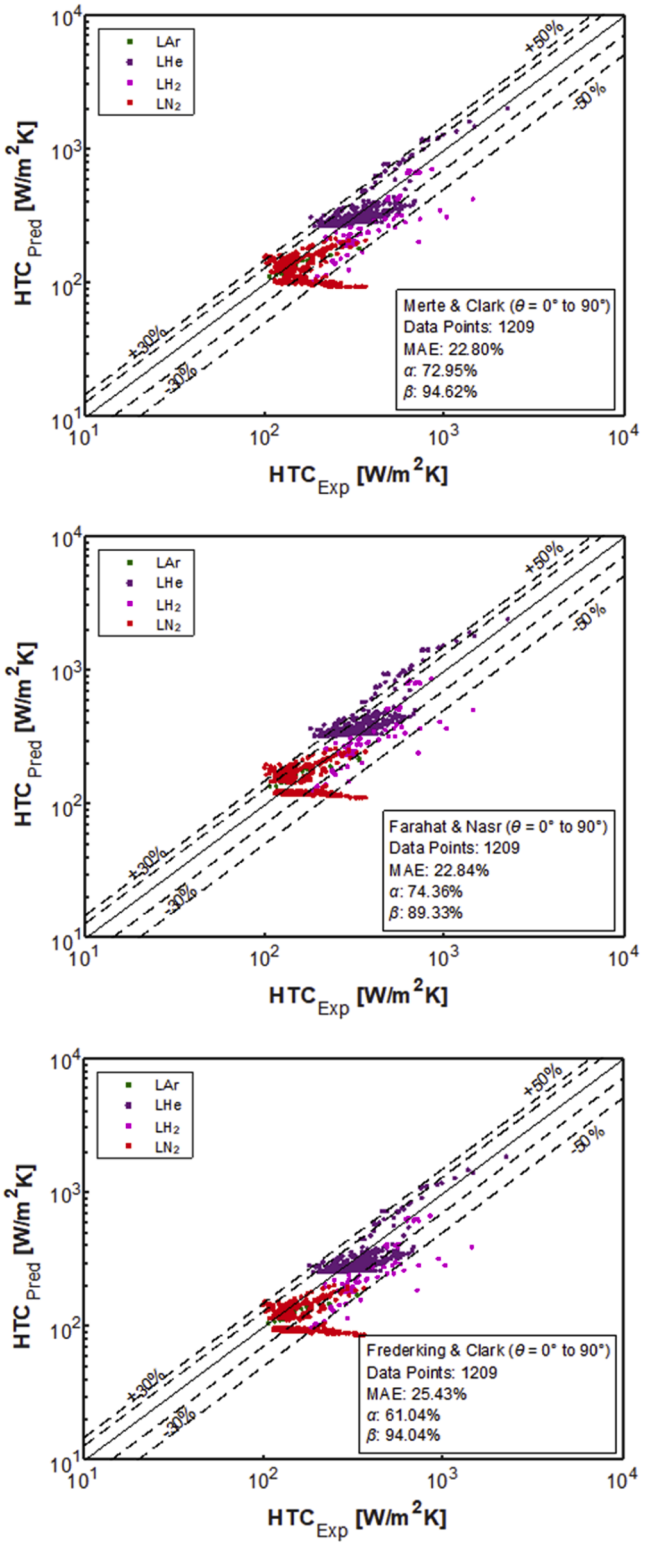

Fig. 14. Best performing prior correlations for all orientations combined showing inferior accuracy compared to that shown in Fig. 12 for the new correlation.

correlation, evidence by a MAE of 11.59 %, compared to MAE values for Farahat and Nasr [48], Sciance et al. [36], and Bromley [31] of 16.98 %, 18.03 %, and 22.12 %, respectively.

These comparative analyses underscore the superior predictive accuracy of the new correlation, positioning it as a robust and reliable predictive tool for both horizontal and vertical orientations in cryogenic pool film boiling.

5.3. Superiority of new correlation over prior correlations

The superiority of the new correlation over existing models in cryogenic pool film boiling heat transfer is evident through several key facets, solidifying its status as a robust and versatile predictor.

One of the primary indicators of its superiority lies in its consistently lowest MAE across both horizontal and vertical orientations, with remarkably low MAEs of 15.47 % and 11.59 %, respectively. Further proof of its superiority comes from comparison of its performance for all orientations from 0° to 90° combined from Fig. 12 to those of best performing prior correlations for the entire range of orientations, namely Merte and Clark [46], Farahat and Nasr [48], and Frederking and Clark [45], as depicted in Fig. 14. Notably, prior correlations show limitations in terms of surface orientation angle. For example, Frederking and Clark's correlation performs best for horizontal orientation but not satisfactory for vertical orientation.

Another key distinguishing attribute of the new correlation is its incorporation of radiation effects, a factor often overlooked in prior studies. Inclusion of the radiation term allows the new correlation to perform exceptionally well at higher wall superheats, where radiation becomes a significant contributor to heat transfer. To elaborate this point, the performance of the new correlation is evaluated for elevated temperatures with wall superheat exceeding 500 K. This comparison shows that the new correlation is the only one performing exceptionally well at elevated temperatures with its MAE of 8.44 % followed by Farahat and Nasr [48], Merte and Clark [46], and Frederking and Clark [45] with their corresponding MAEs of 19.70 %, 31.22 %, and 37.16 %, respectively.

5.4. Summary of statistical results of prior predictive tools

The assessments of all prior correlations have been thoroughly discussed in the preceding sections. This section is dedicated to summarizing these results and providing a comparative overview in a single visual representation. Given that the correlations are evaluated separately for horizontal and vertical orientations, the performance summaries are also segregated. The statistical summaries for horizontal and vertical orientations are provided in Figs. 15 and 16, respectively. Each figure illustrates the results for MAE and the percentages of predictions falling within ±30 % (α) and ±50 % (β) of the data. Lower values of MAE and higher percentages of both α and β indicate better predictive accuracy. It is important to note that results for some correlations with MAEs above 100 % are excluded from these figures to ensure clarity and ease of comparison in the graphs. For a more comprehensive overview, the quantitative comparisons of both the included and skipped correlations are presented in Tables 6 and 7 for the horizontal and vertical orientations, respectively.

While the new correlation is not discussed in detail in this section, its results are incorporated in Figs. 15 and 16 as well as Tables 6 and 7 for direct comparison with prior correlations. The subsequent section will delve into the new correlation and highlight its advantages over the existing ones.

In summary, the superiority of the new correlation is marked by its lowest MAE across different orientations, its applicability to all surface orientations, and its incorporation of radiation effects, collectively establishing it as an effective and versatile predictive tool in the realm of cryogenic pool film boiling heat transfer. Additionally, both the Consolidated Database and new HTC formulation provide a foundation for ongoing PU-BTPFL efforts involving adaptation of machine learning methods, which have shown great potential for correlating data for both flow boiling [79-81] and flow condensation [82]. Equally important is the potential to utilize the Consolidated Database for validation of pool boiling CFD models, capitalizing on recent successes with respect to flow

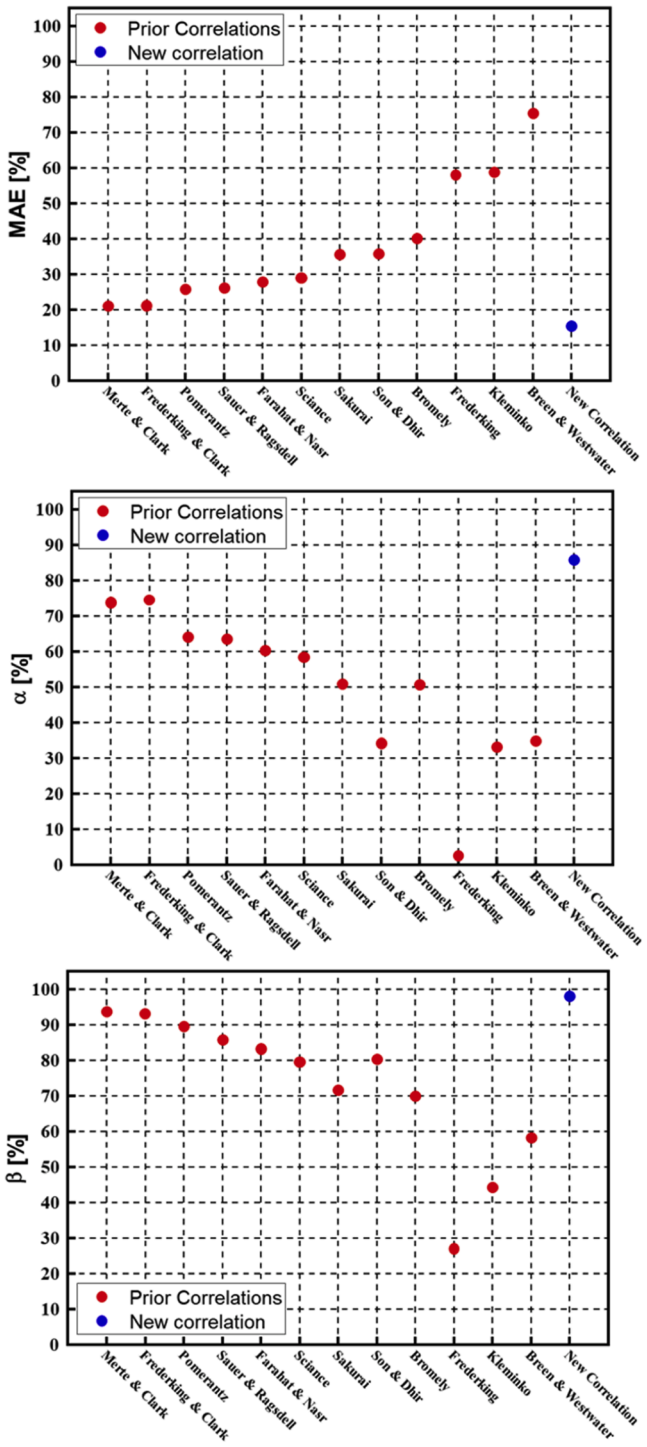

Fig. 15. Summary of predictive performances of all assessed correlations for horizontal surfaces.

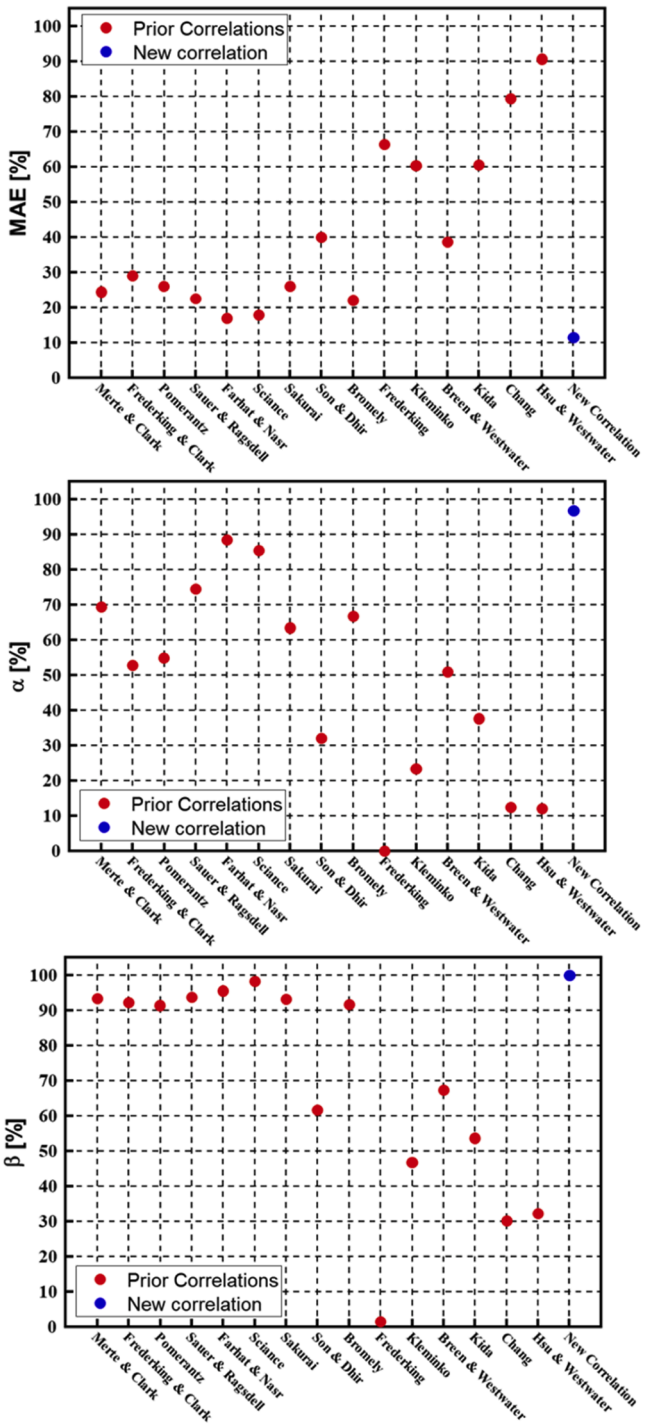

Fig. 16. Summary of predictive performances of all assessed correlations for vertical surfaces.

boiling [83,84].

6. Conclusions

The impetus for this study arises from the notable absence of a robust and comprehensive pool film boiling database for cryogenic fluids. Establishing such a database is imperative for assessing the predictive accuracy of existing models and correlations while also paving the way for the development of a new, more superior predictive methodology. The correlation developed in this study in conjunction with those recently developed for CHF [30], nucleate boiling [85] and both MHF point temperature and heat flux [86] will provide a basis for constructing a complete boiling curve for cryogenic fluids. The key insights derived from this investigation are summarized as follows:

1. The present study undertook a comprehensive exploration of the mechanisms and prevalent trends in pool film boiling, providing valuable insights into the factors influencing the HTC. A compilation of 23 distinct models and correlations was meticulously presented to evaluate their predictive accuracy.

Table 6
Performance summary of all correlations compared to that of the new correlation for flat horizontal surfaces.

	Author(s)	MAE [%]	Predictions within ±30 (α) [%]	Predictions within ±50 (β) [%]	No. of data points
1	Merte & Clark [46]	21.12	73.90	93.70	682
2	Frederking & Clark [45]	21.29	74.63	93.26	682
3	Pomerantz [52]	25.89	64.22	89.59	682
4	Sauer & Ragsdell [26]	26.27	63.64	85.78	682
5	Farhat & Nasr [48]	27.90	60.41	83.28	682
6	Sciance et al. [36]	29.05	58.50	79.62	682
7	Sakurai [37, 38]	35.78	51.03	71.70	682
8	Son & Dhir [58]	35.97	34.31	80.35	682
9	Bromely [31]	40.18	50.73	70.09	682
10	Frederking et al. [41]	58.16	2.64	27.13	682
11	Klimenko [42]	58.92	33.28	44.43	682
12	Breen & Westwater [35]	75.48	34.90	58.36	682
13	Kida et al. [56]	106.74	15.54	30.79	682
14	Chang [29]	136.14	9.53	14.96	682
15	Hsu & Westwater [49]	147.22	9.09	14.96	682
16	Clements & Colver [55]	295.96	0.29	0.44	682
17	Chu [57]	568.59	0	0	682
New Correlation		**15.47**	**85.78**	**98.09**	**682**

Table 7
Performance summary of all correlations compared to that of the new correlation for flat vertical surfaces.

	Author(s)	MAE [%]	Predictions within ±30 (α) [%]	Predictions within ±50 (β) [%]	No. of data points
1	Merte & Clark [46]	24.49	69.44	93.47	337
2	Frederking & Clark [45]	29.10	52.82	92.28	337
3	Pomerantz [52]	26.05	54.90	91.39	337
4	Sauer & Ragsdell [26]	22.59	74.48	93.77	337
5	Farhat & Nasr [48]	16.98	88.43	95.55	337
6	Sciance et al. [36]	18.03	85.46	98.22	337
7	Sakurai [37, 38]	26.08	63.50	93.18	337
8	Son & Dhir [58]	40.10	32.05	61.72	337
9	Bromely [31]	22.12	66.77	91.69	337
10	Frederking et al. [41]	66.43	0	1.48	337
11	Klimenko [42]	60.31	23.44	46.88	337
12	Breen & Westwater [35]	38.68	51.04	67.36	337
13	Kida et al. [56]	60.64	37.69	53.71	337
14	Chang [29]	79.35	12.46	30.27	337
15	Hsu & Westwater [59]	90.68	12.17	32.34	337
16	Clements & Colver [55]	201.08	0	0.59	337
17	Chu [57]	444.41	0	0	337
New Correlation		**11.59**	**96.74**	**100**	**337**

2. Through application of stringent criteria, a Consolidated Cryogenic Pool Film Boiling Database was curated, comprising 1209 data points gathered for four cryogenic fluids: LAr, LHe, LH_2, and LN_2. Most of the data (56.4 %) pertain to the horizontal orientation ($\theta = 0^\circ$) and 27.9 % to the vertical orientation (90°). The remaining 15.7 % correspond to other in-between orientations (30° and 60°).
3. A detailed assessment of prior models and correlations revealed a spectrum of inaccuracies for different orientations. These predictive tools were presented in a uniform formulation which helped in combining the main attributes of prior correlations to develop the new correlation.
4. Leveraging the Consolidated Database, a new universal correlation for cryogenic pool film boiling HTC was formulated. The new correlation outperformed all previous models and correlations by achieving the lowest MAE for every orientation angle. The corresponding MAEs of the new correlation for different orientations were 15.47 % ($\theta = 0^\circ$), 11.59 % (90°), 7.92 % (30°), and 3.78 % (60°).
5. The new correlation not only achieved the lowest MAEs but also showed tremendous performance at elevated temperatures because of the inclusion of radiation effects. Moreover, the addition of orientation term (θ) renders the new correlation highly robust in tackling all orientations.
6. Researchers historically favored geometries like tubes and spheres, but future emphasis should shift to studying flat surfaces for a nuanced understanding of cryogenic pool film boiling. Addressing data gaps, especially for cryogens like LAr, LO_2, LCH_4, and para-hydrogen, is crucial for a comprehensive grasp of the underlying fluid physics. Balancing datasets across surface orientations, further exploring elevated conditions, and considering reduced gravity environments (microgravity, Lunar, and Martian) will contribute to a comprehensive future understanding of cryogenic pool film boiling.

CRediT authorship contribution statement

Faraz Ahmad: Writing – review & editing, Writing – original draft, Validation, Software, Methodology, Investigation, Formal analysis, Data curation, Conceptualization. **Michael Meyer:** Writing – review & editing, Supervision, Project administration, Methodology, Funding acquisition, Conceptualization. **Jason Hartwig:** Writing – review & editing, Writing – original draft, Supervision, Project administration, Methodology, Investigation, Funding acquisition, Conceptualization. **Issam Mudawar:** Writing – review & editing, Writing – original draft, Supervision, Project administration, Methodology, Investigation, Funding acquisition, Formal analysis, Conceptualization.

Declaration of competing interest

The authors declare the following financial interests/personal relationships which may be considered as potential competing interests: Issam Mudawar reports financial support was provided by NASA. Issam Mudawar reports a relationship with NASA that includes: funding grants. If there are other authors, they declare that they have no known competing financial interests or personal relationships that could have appeared to influence the work reported in this paper.

Data availability

The data that has been used is confidential.

Acknowledgment

The authors are grateful for financial support of the National Aeronautics and Space Administration (NASA) Small Business Technology Transfer (STTR) program under a subcontract from MTS Inc. Phase II contract 80NSSC23CA009.

References

[1] I. Mudawar, Recent advances in high-flux, two-phase thermal management, J Therm Sci Eng Appl 5 (2013) 021012.
[2] T.J. LaClair, I. Mudawar, Thermal transients in a capillary evaporator prior to the initiation of boiling, Int. J. Heat Mass Transf. 43 (2000) 3937–3952.
[3] G. Liang, I. Mudawar, Pool boiling critical heat flux (CHF) – part 2: assessment of models and correlations, Int. J. Heat Mass Transf. 117 (2018) 1368–1383.
[4] I. Mudawar, R.A. Houpt, Mass and momentum transport in smooth falling liquid films laminarized at relatively high Reynolds numbers, Int. J. Heat Mass Transf. 36 (1993) 3437–3448.
[5] C.O. Gersey, I. Mudawar, Effects of heater length and orientation on the trigger mechanism for near-saturated flow boiling critical heat flux - II. Critical heat flux model, Int. J. Heat Mass Transf. 38 (1995) 643–654.
[6] S. Mukherjee, I. Mudawar, Pumpless loop for narrow channel and micro-channel boiling from vertical surfaces, J. Electron. Packag. 125 (2003) 431–441.
[7] M.E. Johns, I. Mudawar, An ultra-high power two-phase jet-impingement avionic clamshell module, J. Electron. Packag. 118 (1996) 264–270.
[8] W.P. Klinzing, J.C. Rozzi, I. Mudawar, Film and transition boiling correlations for quenching of hot surfaces with water sprays, J. Heat Treat. 9 (1992) 91–103.
[9] M.K. Sung, I. Mudawar, Single-phase and two-phase heat transfer characteristics of low temperature hybrid micro-channel/micro-jet impingement cooling module, Int. J. Heat Mass Transf. 51 (2008) 3882–3895.
[10] M.K. Sung, I. Mudawar, Single-phase and two-phase hybrid cooling scheme for high-heat-flux thermal management of defense electronics, J. Electron. Packag. 131 (2009) 021013.
[11] S.W. Churchill, R. Usagi, A general expression for the correlation of rates of transfer and other phenomena, AIChE J 18 (1972) 1121–1128.
[12] T.N. Tran, M.W. Wambsganss, D.M. France, Small circular- and rectangular-channel boiling with two refrigerants, Int. J. Multiph. Flow 22 (1996) 485–498.
[13] K.A. Triplett, S.M. Ghiaasiaan, S.I. Abdel-Khalik, A. LeMouel, B.N. McCord, Gas-liquid two-phase flow in microchannels Part II: void fraction and pressure drop, Int. J. Multiph. Flow 25 (1999) 395–410.
[14] S.-M. Kim, I. Mudawar, Universal approach to predicting saturated flow boiling heat transfer in mini/micro-channels–Part I. Dryout incipience quality, Int. J. Heat Mass Transf. 64 (2013) 1226–1238.
[15] X. Li, W. Wei, R. Wang, Y. Shi, Numerical and experimental investigation of heat transfer on heating surface during subcooled boiling flow of liquid nitrogen, Int. J. Heat Mass Transf. 52 (2009) 1510–1516.
[16] R. Zhuan, W. Wang, Flow pattern of boiling in micro-channel by numerical simulation, Int. J. Heat Mass Transf. 55 (2012) 1741–1753.
[17] C.R. Kharangate, I. Mudawar, Review of computational studies on boiling and condensation, Int. J. Heat Mass Transf. 108 (2017) 1164–1196.
[18] S. Kim, J. Lee, J. Hartwig, I. Mudawar, Computational investigation of vertical upflow boiling of liquid nitrogen and effects of bubble collision dispersion force, Int. J. Heat Mass Transf. 203 (2023) 123780.
[19] S.-M. Kim, I. Mudawar, Theoretical model for annular flow condensation in rectangular micro-channels, Int J Heat Mass Transf 55 (2012) 958–970.
[20] E.W. Lemmon, I.H. Bell, M.L. Huber, M.O. McLinden, NIST standard reference database 23: reference fluid thermodynamic and transport properties-REFPROP, Version 10.0, National Institute of Standards and Technology, Standard Reference Data Program, Gaithersburg (2018).
[21] V. Ganesan, R. Patel, J. Hartwig, I. Mudawar, Review of databases and correlations for saturated flow boiling heat transfer coefficient for cryogens in uniformly heated tubes, and development of new consolidated database and universal correlations, Int. J. Heat Mass Transf. 179 (2021) 121656.
[22] C.R. Class, J.R. DeHaan, M. Piccone, R.B. Cost, Boiling heat transfer to liquid hydrogen from flat surfaces, in: Advances in Cryogenic Engineering: Proc. 1959 Cryogenic Eng. Conf., Berkeley, California, Sep. 2–4, 1959, pp. 254–261.
[23] I. Kumar, A.K. Roy, A. Hens, Effect of pressure variations on film boiling characteristics of liquid nitrogen, Phys. Fluids 35 (2023) 102101.
[24] C.E. Price, Film Boiling from Inclined Flat Surfaces (1969), Masters Thesis, U. Missouri-Rolla, 1969.
[25] M.W. Scheiwe, U. Hartmann, Heat transfer from warm plates of cryobiologic interest to liquid nitrogen, in: Proc. 9th Int. Cryogenic Eng. Conf., Kobe, Japan, May 11–14, 1982, pp. 81–84.
[26] H.J. Sauer Jr, K.M. Ragsdell, Film pool boiling of nitrogen from flat surfaces, in: Proc. 1970 Cryogenic Eng. Conf., Boulder, Colorado, June 17–17, 1970, pp. 412–415.
[27] E.G. Brentari, Nuclear and film pool boiling design correlations for O_2, N_2, H_2 and He, Adv. Cryog. Eng. 10 (1965) 325–341.
[28] P.J. Berenson, Film-boiling heat transfer from a horizontal surface, J. Heat Transf. 83 (1961) 351–356.
[29] Y.P. Chang, Wave theory of heat transfer in film boiling, J. Heat Transf. 81 (1959) 1–8.
[30] R. Patel, M. Meyer, J. Hartwig, I. Mudawar, Review of cryogenic pool boiling critical heat flux databases, assessment of models and correlations, and development of new universal correlations, Int J Heat Mass Transf 190 (2022) 122579.
[31] L.A. Bromley, Heat transfer in stable film boiling, US Atomic Energy Commission, Technical Information Division (1949) 2295.
[32] W.M. Rohsenow, J.P. Hartnett, Y.I. Cho, Handbook of Heat Transfer, 3rd ed., McGraw-Hill, 1998.
[33] W. Nusselt, Die oberflachenkondensation des wasserdamphes, VDI-Zs 60 (1916) 541.
[34] K. Nishikawa, T. Ito, T. Kuroki, K. Matsumoto, Pool film boiling heat transfer from a horizontal cylinder to saturated liquids, Int. J. Heat Mass Transf. 15 (1972) 853–862.
[35] B.P. Breen, J.W. Westwater, Effect of diameter of horizontal tubes on film boiling heat transfer, Chem. Eng. Prog. 58 (1962) 67–72.
[36] C.T. Sciance, C.P. Colver, C.M. Sliepcevich, Film boiling measurements and correlation for liquefied hydrocarbon gases, Chem. Eng. Prog. Symp. Ser. 63 (1967) 115–119.
[37] A. Sakurai, M. Shiotsu, K. Hata, A general correlation for pool film boiling heat transfer from a horizontal cylinder to subcooled liquid: part 1 - A theoretical pool film boiling heat transfer model including radiation contributions and its analytical solution, J. Heat Transf. 112 (1990) 430–440.
[38] A. Sakurai, M. Shiotsu, K. Hata, A general correlation for pool film boiling heat transfer from a horizontal cylinder to subcooled liquid: part 2 - Experimental data for various liquids and its correlation, J. Heat Transf. 112 (1990) 441–450.
[39] K.J. Baumeister, T.D. Hamill, Laminar Flow Analysis of Film Boiling from a Horizontal Wire, NASA Technical Note, 1967.
[40] K.J. Baumeister, T.D. Hamill, Film boiling from a thin wire as an optimal boundary-value process, J. Mech. Eng. 89 (1967) 79–88.
[41] T.H.K. Frederking, Y. Wu, B.W. Clement, Effects of interfacial instability on film boiling of saturated liquid helium I above a horizontal surface, AIChE J 12 (1966) 238–244.
[42] V.V. Klimenko, Film boiling on a horizontal plate—New correlation, Int J Heat Mass Transf 24 (1981) 69–79.
[43] N. Zuber, Hydrodynamic aspects of boiling heat transfer, United States Atomic Energy Commission Technical Report no. 4439, 1959.
[44] S.C. Lin, Effect of Inclination On Film Boiling, U. Missouri-Rolla, 1970 masters thesis.
[45] T.H.K. Frederking, J.A. Clark, Natural convection film boiling on a sphere, in: Proc. 1962 Cryogenic Eng. Conf., Los Angeles, California, August 14–16, 1962, pp. 501–506.
[46] H. Merte Jr, J.A. Clark, Boiling heat transfer with cryogenic fluids at standard, fractional, and near-zero gravity, J. Heat Transf. 86 (1964) 351–358.
[47] J. Ruzicka, Heat transfer to boiling nitrogen, in: Proc. Mtg. of Comm. I of Int. Inst. Refrig., Delft, Nerherlands, 1959, p. 323.
[48] M.M. Farahat, Natural convection film boiling from spheres to saturated liquids, an integral approach, Int. J. Heat Mass Transf. 21 (1978) 256–258.
[49] Y.-Y. Hsu, J.W. Westwater, Film boiling from vertical tubes, AIChE J 4 (1958) 58–62.
[50] Y.P. Chang, A theoretical analysis of heat transfer in natural convection and in boiling, Trans. ASME 79 (1957) 1501–1509.
[51] S.S. Kutateladze, Heat Transfer in Condensation and Boiling, US Atomic Energy Commission, 1959. Technical Report.
[52] M.L. Pomerantz, Film boiling on a horizontal tube in increased gravity fields, J. Heat Transf. 86 (1964) 213–218.
[53] C.A. Heath, C.P. Costello, Some effects of geometry, orientation, and acceleration on pool film boiling of organic fluids, J. Eng. Ind. 88 (1966) 17–23.
[54] V.J. Flanigan, A Study of Film Boiling of Liquid Nitrogen and Liquid Argon Over a Wide Pressure Range With Cylindrical heaters, Masters Thesis, U. Missouri-Rolla, 1967.
[55] L.D. Clements, C.P. Colver, Generalized correlation for film boiling, J. Heat Transf. 94 (1972) 324–326.
[56] M. Kida, Y. Kikuchi, O. Takahashi, I. Michiyoshi, Pool-boiling heat transfer in liquid nitrogen, J. Nucl. Sci. Technol. 18 (1981) 501–513.
[57] T.Y. Chu, A correlational approach to turbulent saturated film boiling, J. Heat Transf. 115 (1993) 993–997.
[58] G. Son, V.K. Dhir, Numerical simulation of film boiling near critical pressures with a level set method, J Heat Transfer 120 (1998) 183–192.
[59] A. Rohatgi, WebPlotDigitizer, https://automeris.io, WebPlotDigitizer2018.
[60] R.W. Graham, R.C. Hendricks, R.C. Ehlers, An experimental study of the pool heating of liquid hydrogen in the subcritical and supercritical pressure regimes over a range of accelerations, Adv. Cryog. Eng. 10 (1965) 342–352.
[61] D.N. Lyon, Boiling heat transfer and peak nucleate boiling fluxes in saturated liquid helium between the lamda and critical temperatures, Adv. Cryog. Eng. 10 (1965) 371.
[62] P.C. Wayner Jr, S.G. Bankoff, Film boiling of nitrogen with suction on an electrically heated porous plate, AIChE J 11 (1965) 59–64.
[63] R.D. Cummings, J.L. Smith, Boiling Heat Transfer to Liquid helium, Liquid Helium Technology, Pergamon Press, 1966, pp. 85–95.
[64] J.A. Clark, E.W. Lewis, H. Merte Jr, Boiling of Liquid Nitrogen in Reduced Gravity Fields With Subcooling, NASA Technical Note NASA-CR-98248, 1967.
[65] H. Merte, Incipient and Steady Boiling of Liquid Nitrogen and Liquid Hydrogen Under Reduced Gravity, Dept. Mech. Eng. report, Univ. Michigan, 1970.
[66] V.I. Deev, V.E. Keilin, I.A. Kovalev, A.K. Kondratenko, V.I. Petrovichev, Nucleate and film pool boiling heat transfer to saturated liquid helium, Cryogenics (Guildf) 17 (1977) 557–562.

[67] V.A. Grigoriev, V.V. Klimenko, Y.M. Pavlo, Y.V. Ametistov, A.V. Klimenko, Characteristic curve of helium pool boiling, Cryogenics (Guildf) 17 (1977) 155–156.
[68] H. Ogata, Heat transfer to boiling helium from machined and chemically treated copper surfaces, Adv. Cryog. Eng. 27 (1981) 309–317.
[69] V.V. Klimenko, A.G. Shelepen, Film boiling on a horizontal plate—A supplementary communication, Int. J. Heat Mass Transf. 25 (1982) 1611–1613.
[70] M.W. Scheiwe, U. Hartmann, Heat transfer from warm plates of cryobiologic interest to liquid nitrogen, in: Proc. 9th Int. Cryog. Eng. Conf., Kobe, Japan, May 11–14, 1982, pp. 81–84.
[71] S. Nishio, Study on minimum heat-flux point during boiling heat transfer on horizontal plates, Nippon Kikai Gakkai Ronbunshu, B Hen 51 (1985) 582–590.
[72] G.R. Chandratilleke, S. Nishio, H. Ohkubo, Pool boiling heat transfer to saturated liquid helium from coated surface, Cryogenics (Guildf) 29 (1989) 588–592.
[73] S. Nishio, G.R. Chandratilleke, Steady-state pool boiling heat transfer to saturated liquid helium at atmospheric pressure, JSME Int. J. Ser. B - Fluids Therm. Eng. 32 (1989) 639–645.
[74] S.M. Kozlov, S.V. Nozdrin, Heat transfer and boundaries of its regimes during hydrogen boiling at different metallic surfaces, Cryogenics (Guildf) 32 (1992) 245–248.
[75] H. Ogata, H. Mori, Steady state heat transfer in transition boiling of helium on copper surfaces, Cryogenics (Guildf) 33 (1993) 640–642.
[76] A. Iwamoto, R. Maekawa, T. Mito, J. Yamamoto, Steady state heat transfer characteristics in He I with different surface area, Adv. Cryog. Eng. 43 (1998) 1481–1487.
[77] T. Jin, J. Hong, H. Zheng, K. Tang, Z. Gan, Measurement of boiling heat transfer coefficient in liquid nitrogen bath by inverse heat conduction method, J. Zhejiang Univ. -Sci A 10 (2009) 691–696.
[78] B.V. Balakin, M.I. Delov, K.V. Kutsenko, A.A. Lavrukhin, O.V. Zhdaneev, Heat transfer from Ni–W tapes in liquid nitrogen at different orientations in the field of gravity, Cryogenics (Guildf) 65 (2015) 5–9.
[79] Y. Qiu, D. Garg, L. Zhou, C.R. Kharangate, S. Kim, I. Mudawar, An artificial neural network model to predict mini/micro-channels saturated flow boiling heat transfer coefficient based on universal consolidated data, Int. J. Heat Mass Transf. 149 (2020) 119211.
[80] Y. Qiu, D. Garg, S. Kim, I. Mudawar, C.R. Kharangate, Machine learning algorithms to predict flow boiling pressure drop in mini/micro-channels based on universal consolidated data, Int. J. Heat Mass Transf. 178 (2021) 121607.
[81] I. Mudawar, S.J. Darges, V.S. Devahdhanush, Prediction technique for flow boiling heat transfer and critical heat flux in both microgravity and earth gravity via artificial neural networks (ANNs), Int. J. Heat Mass Transf. 220 (2024) 124998.
[82] L. Zhou, D. Garg, Y. Qiu, C.R. Kharangate, S. Kim, I. Mudawar, Machine learning algorithms to predict flow condensation heat transfer coefficient in mini/micro-channel utilizing universal data, Int. J. Heat Mass Transf. 162 (2020) 120351.
[83] I. Mudawar, J. Lee, Experimental and computational investigation into hydrodynamic and heat transfer characteristics of subcooled flow boiling on the International Space Station, Int. J. Heat Mass Transf. 207 (2023) 124000.
[84] I. Mudawar, S. Kim, J. Lee, A coupled level-set and volume-of-fluid (CLSVOF) method for prediction of microgravity flow boiling with low inlet subcooling on the International Space Station, Int. J. Heat Mass Transf. 217 (2023) 124644.
[85] F. Ahmad, S. Kim, M. Meyer, J. Hartwig, I. Mudawar, Saturated nucleate pool boiling of cryogenic fluids: review of databases, assessment of existing models and correlations, and development of new universal correlation, Int J Heat Mass Transf 231 (2024) 125807.
[86] F. Ahmad, M. Meyer, J. Hartwig, I. Mudawar, Development of new universal correlations for minimum heat flux point for saturated pool boiling of cryogens, Int J Heat Mass Transf 234 (2024) 126099.